

# Covariant Holographic Entanglement Entropy Inversion to Reconstruct Bulk Geometry

Ji-Seong Chae<sup>†1</sup>

<sup>†</sup>*Department of Physics, Hanyang University, Seoul 04763, Korea*

## Abstract

We present an analytic inversion of covariant holographic entanglement entropy beyond equal-time inversion, in which only one effective radial coefficient remains after the radial gauge and transverse density are fixed. The formula reconstructs the stationary radial metric block probed by the corresponding HRT geodesics, including a nontrivial spatial warp factor and the stationary shift associated with frame dragging. In this sector, the renormalized interval entropy  $S(\Delta t, \Delta x)$  is an on-shell Hamilton–Jacobi functional. Its endpoint derivatives determine the conserved charges of the corresponding extremal geodesic, and their ratio characterizes the projective class of the endpoint covector associated with the boundary interval,  $\kappa = E/J = -\partial_{\Delta t} S_{\text{ren}}/\partial_{\Delta x} S_{\text{ren}}$ . For each fixed  $\kappa$ , the entropy data define an Abel-type reconstruction of a radial metric block. A single classical geometry is obtained only when the reconstructions from different fixed- $\kappa$  families agree as functions of one common radial coordinate. This cross-family compatibility condition is the integrability condition of the covariant inverse problem. The analysis is restricted to the classical Hubeny–Rangamani–Takayanagi(HRT) area term.

arXiv:2605.16459v3 [hep-th] 1 Jun 2026

---

<sup>1</sup>jiseongchae17@gmail.com

# Contents

<b>1</b>	<b>Introduction</b>	<b>1</b>
<b>2</b>	<b>Holographic entanglement entropy and static inversions</b>	<b>4</b>
2.1	From Ryu–Takayanagi to Hubeny–Rangamani–Takayanagi . . . . .	4
2.2	Bilson’s static geodesic inversions . . . . .	5
2.3	Bilson’s strip inversion and the equal-time obstruction . . . . .	7
2.4	From static probes to covariant HRT . . . . .	9
<b>3</b>	<b>Inversion formula from covariant holographic entanglement entropy</b>	<b>10</b>
3.1	Stationary metric class and Hamilton–Jacobi variables . . . . .	10
3.2	Characteristic Abel inversion and metric reconstruction . . . . .	12
3.3	Causal readout of the reconstructed metric . . . . .	16
3.4	Admissibility conditions and higher-dimensional extension . . . . .	17
<b>4</b>	<b>Examples</b>	<b>23</b>
4.1	Pure AdS, rotating BTZ, and a static warped geometry . . . . .	23
4.2	A boosted Einstein–scalar black brane . . . . .	31
4.3	A higher-dimensional strip degeneracy . . . . .	36
<b>5</b>	<b>Discussion</b>	<b>38</b>

## 1 Introduction

A central question in holography is not only how a known bulk geometry computes boundary observables, but also when boundary data determine the geometry in the first place. In the anti-de Sitter/conformal field theory (AdS/CFT) correspondence, the bulk radial direction is emergent, and reconstructing the metric from field-theory data is therefore a concrete form of the spacetime-emergence problem [1–3]. Entanglement entropy is especially suited to this question because it has a direct geometric representation. The Ryu–Takayanagi (RT) prescription relates the entropy of a boundary spatial region in a static state to the area of a bulk minimal surface [4], while the Hubeny–Rangamani–Takayanagi (HRT) prescription replaces this minimal surface by a Lorentzian extremal surface in time-dependent or stationary non-static geometries [5]. These prescriptions are usually used in the forward direction. The inverse problem asks whether the same geometric relation can be reversed.

The present study addresses this inverse problem beyond the usual one-function blackening-factor setting. We develop an analytic inversion of covariant holographic entanglement entropy that reconstructs the effective radial block seen by a symmetry-reduced HRT problem. In the stationary homogeneous three-dimensional sector, this means reconstructing not only a blackening function but also a nontrivial spatial warp factor and a stationary shift. The stationary shift is the local frame-dragging profile in a rotating geometry. Thus the object reconstructed from entanglement is the stationary Lorentzian block, which controls both distances and the projected light cone.

The motivation comes from a limitation of equal-time entanglement. Equal-time RT surfaces probe the spatial geometry effectively, but they do not by themselves carry the full information contained in a stationary Lorentzian metric. A static metric with more than one radial function already illustrates the issue: a one-parameter family of equal-time intervals cannot generally separate all metric functions without additional input. In a rotating geometry the problem is sharper. The shift, or frame-dragging term, is invisible to a purely spatial slice but is visible to covariant HRT curves whose endpoints have both time and spatial separation. The time separation of the interval is therefore an independent part of the covariant boundary data, rather

than a redundant extension of the equal-time RT setup. It supplies the second Hamilton–Jacobi direction needed to recover the stationary block.

The static reference point for this problem is the work of Hammersley and Bilson. Hammersley used boundary information associated with geodesics to extract metric data in asymptotically anti-de Sitter spacetimes [6, 7]. Bilson then gave explicit Abel-type inversions in static, highly symmetric geometries, using spacelike geodesic lengths and null-geodesic endpoint data to recover metric functions [8, 9]. These constructions are the closest analytic predecessors of the present work. A recent rule-based reconstruction from entanglement data has also pushed this static program beyond the metric alone by inferring thermodynamic and matter-sector data after a gravitational ansatz is imposed [10]. These works show that the amount and type of boundary data must match the number of independent radial functions. For the present problem, however, their static setting is insufficient: it contains no stationary shift and no analogue of the cross-family compatibility condition that appears below.

Several other reconstruction programs address neighbouring aspects of the same question. Light-cone cuts and bulk-cone singularities use singularities of boundary correlators to recover causal structure, and in favorable cases the conformal metric [11–13]. Hamilton–Kabat–Lifschytz–Lowe (HKLL) reconstruction expresses bulk fields in terms of boundary operators once the background geometry is known [14], while holographic renormalization reconstructs the near-boundary expansion from sources and one-point functions [15]. Kinematic space, differential entropy, and hole-ographic constructions organize families of intervals and geodesics into an integral-geometric description of bulk curves and distances [16–19]. Bit threads and entanglement wedge reconstruction provide global and operator-algebraic ways of understanding the same RT/HRT data [20, 21]. These approaches are complementary to the present one. Here the input is the covariant interval HRT length itself, and the output is the local radial block of the metric in the symmetry-reduced sector.

There has also been substantial progress on reconstructing metric information from other boundary observables. Metric data can be constrained from boundary stress tensors and holographic renormalization [15], from correlator singularities and bulk-cone data [11, 12], from Wilson loops [22], and from complexity in black-hole geometries [23, 24]. Modular Hamiltonians and their algebra have also been used to probe emergent spacetime structure [25]. Boundary entanglement has been used directly in several metric-reconstruction settings, including reconstructions from boundary entanglement data, bulk-distance information, and related finite-depth probes of the bulk [16, 26, 27]. Perturbative minimal-surface variation methods recover metric perturbations from variations of area data around a reference background [28, 29], while recent numerical or data-driven RT inversions reconstruct static isotropic or one-function ansatzes from entanglement data [30, 31]. Inverse-scattering approaches reconstruct metric information from boundary two-point functions and bulk wave equations [32]. A complementary analytic direction uses pole-skipping points, namely the discrete momentum-space locations where boundary Green’s functions become ambiguous, as boundary data for metric reconstruction. Recent work has shown that the near-horizon metric data of static planar black holes can be reconstructed from such pole-skipping points by solving linear equations, and that the resulting data obey universal algebraic constraints [33, 34]. The present construction differs from these in three ways: it is analytic rather than numerical, covariant rather than equal-time, and reconstructs the stationary shift together with the radial and spatial metric functions.

The broader physical background is the idea that spacetime connectivity and geometry are encoded in entanglement. This idea appears in many forms, from tensor-network and entanglement-renormalization pictures to the relation between entanglement and black-hole interiors [35–40]. Holographic entanglement entropy and its covariant, quantum, and mixed-state refinements have made this relation precise in several regimes [41–48]. The present work focuses on a more specific and more constructive question: within a symmetry-reduced classical HRT sector, which metric functions are determined by the interval entropy, and what consistency

conditions must the entropy satisfy to come from one classical geometry?

The rotating case gives a clear physical interpretation. In the Bañados–Teitelboim–Zanelli (BTZ) family, rotation is encoded on the boundary by the left–right asymmetric thermal scales and in the bulk by the stationary shift [49–51]. More general rotating or hairy anti–de Sitter black holes separate global thermodynamic data from local radial structure: a horizon angular velocity is a single number, whereas a frame-dragging function is a radial profile. Earlier discussions of rotating anti–de Sitter black holes emphasize their thermodynamics and boundary interpretation [52, 53]; more recent semiclassical rotating examples show that rotation and hair can coexist in ways that are not captured by pure BTZ kinematics alone [54]. These examples motivate an inverse question naturally phrased in terms of covariant entanglement: can the interval data reconstruct the radial profile of frame dragging and identify the causal structures associated with rotation?

Within the stationary homogeneous three-dimensional sector, and more generally for the effective radial block of any HRT problem that reduces to a one-dimensional radial variational problem, the answer is constructive. The renormalized interval length

$$L(\Delta t, \Delta x) = 4G_N S_{\text{ren}}(\Delta t, \Delta x)$$

is treated as an on-shell Hamilton–Jacobi functional. Its endpoint derivatives give the conserved energy and momentum of the HRT geodesic. Their ratio defines a characteristic parameter  $\kappa$ , and the inverse spatial momentum defines a turning-point variable. For each fixed  $\kappa$ , the entropy data define an Abel problem. The nontrivial step is that the candidate reconstructions obtained at different values of  $\kappa$  must agree as functions of one common radial coordinate. This cross-family compatibility condition is the integrability condition of the covariant inverse problem.

When the condition holds, the formula reconstructs the effective radial metric block. In the three-dimensional stationary case this block is the physical metric block itself, and the reconstructed functions determine the projected local light cone,

$$\kappa_{\pm}(z) = -v(z) \pm \sqrt{f(z)/h(z)}.$$

The roots have a direct causal meaning. Their midpoint is the frame-dragging profile, their separation gives the opening of the projected cone, their coalescence identifies the horizon generator, and a zero crossing identifies the stationary-limit surface. Thus the covariant interval entropy determines both radial distances and the local tilt of the stationary causal structure.

The same formulation also clarifies what is not being claimed. The formula does not reconstruct an arbitrary bulk spacetime. It applies when the HRT problem has been reduced, by symmetry and a radial gauge choice, to metric functions of one holographic coordinate. In higher-dimensional strip problems, the formula reconstructs the density-dressed block seen by the strip; the undressed metric is recovered only if the transverse area density is fixed by symmetry or separated by additional region data. In time-dependent states, such as thin-shell quenches, the HRT length depends on the center time of the interval, and the stationary Hamilton–Jacobi charges are no longer globally conserved. Failure of the integrability conditions indicates that the supplied entropy data do not belong to the assumed radial HRT sector.

The examples are chosen to make these statements explicit. Pure anti–de Sitter space fixes the normalization of the Abel variable and radial coordinate. Rotating BTZ starts from the chiral thermal conformal-field-theory entropy and reconstructs the stationary radial block, including the shift. A static warped example shows why nonzero fixed- $\kappa$  families are needed even without rotation. A boosted Einstein–scalar black brane gives a non-BTZ stationary geometry with matter-supported structure and separates metric reconstruction from matter reconstruction. A higher-dimensional strip example exhibits the transverse-density ambiguity directly, and a thin-shell example shows how time dependence obstructs a stationary interpretation.

The result can be summarized as follows. On a smooth HRT branch, in a symmetry-reduced radial sector, the covariant interval entropy determines an effective radial block if and only if the characteristic Abel data satisfy the algebraic, differential, positivity, asymptotic, and cross-family consistency conditions derived below. In the three-dimensional stationary case this effective block gives the physical functions  $f(z), h(z), v(z)$  and the projected light-cone roots. In higher-dimensional strip reductions it gives the density-dressed block unless additional data separate the transverse density.

The study is organized as follows. Section 2 reviews holographic entanglement entropy, the static Abel inversions of Hammersley and Bilson, and the limitation of equal-time data. Section 3 develops the covariant Hamilton–Jacobi variables, derives the Abel kernels, states the reconstruction formula, and identifies the admissibility conditions. Section 4 works out the explicit checks and examples described above. Section 5 discusses limitations, dynamical interpretation, quantum and Rényi corrections, and possible extensions of the analytic formula.

## 2 Holographic entanglement entropy and static inversions

### 2.1 From Ryu–Takayanagi to Hubeny–Rangamani–Takayanagi

For a static asymptotically anti-de Sitter (AdS) bulk spacetime, the Ryu–Takayanagi (RT) prescription assigns to a spatial boundary region  $A$  the entropy

$$S(A) = \frac{\text{Area}(\gamma_A)}{4G_N}, \quad (1)$$

where  $\gamma_A$  is the bulk codimension-two minimal surface anchored on  $\partial A$  and homologous to  $A$  [4]. In AdS<sub>3</sub> the surface is a spacelike geodesic, and the area in (1) is replaced by a length. We write

$$L_{\text{ren}}(A) = 4G_N S_{\text{ren}}(A), \quad (2)$$

for the renormalized length after the universal near-boundary divergence has been subtracted.

For a spacelike codimension-two surface  $\mathcal{X}_A$  in a Lorentzian bulk, the two independent normal directions may be chosen as null vectors  $k_+^\mu$  and  $k_-^\mu$ . The corresponding null expansions

$$\theta_{(\pm)} = \frac{1}{\sqrt{\gamma}} \mathcal{L}_{k_\pm} \sqrt{\gamma} \quad (3)$$

measure the first-order change of the area density when  $\mathcal{X}_A$  is displaced along these two null normal directions. The covariant prescription of Hubeny, Rangamani and Takayanagi (HRT) replaces the RT minimal surface on a Euclidean or time-reflection-symmetric slice by a Lorentzian extremal surface satisfying

$$\theta_{(+)}|_{\mathcal{X}_A} = 0, \quad \theta_{(-)}|_{\mathcal{X}_A} = 0, \quad (4)$$

with  $\partial\mathcal{X}_A = \partial A$ . Equivalently, the area is stationary under arbitrary normal deformations of  $\mathcal{X}_A$ . Among the homologous extremal surfaces satisfying this condition, one chooses the surface of least area.

This distinction is essential in Lorentzian signature. On a Euclidean or time-reflection-symmetric slice the RT problem is a genuine minimization problem within a Riemannian geometry. In a general Lorentzian spacetime, however, deformations of a spacelike surface include timelike normal directions, and the area functional is not minimized in the same positive-definite sense. The correct local variational condition is extremality, not minimization on an arbitrarily chosen time slice. Consequently, in a stationary but non-static geometry, such as a rotating background with  $g_{tx} \neq 0$ , one cannot in general obtain the HRT surface by restricting to a constant-time slice and minimizing there. That shortcut is justified only when a symmetry,

for example time reflection symmetry in a static spacetime, guarantees that the time-normal variation also vanishes.

For later use it is helpful to separate three statements that are sometimes conflated. First, (1) is a forward formula: given the metric, one computes  $\gamma_A$  or  $\mathcal{X}_A$ . Second, the inverse problem asks whether the boundary function  $S_{\text{ren}}(A)$  determines the metric. Third, in a non-static stationary geometry the relevant boundary datum is not only  $S_{\text{ren}}(0, \Delta x)$  but the covariant interval entropy  $S_{\text{ren}}(\Delta t, \Delta x)$  on a spacelike domain. The rotating Bañados–Teitelboim–Zanelli (BTZ) geometry gives a simple illustration: the HRT extremal geodesic is obtained most cleanly by using the local AdS<sub>3</sub> map, and although the interval endpoints can be at equal boundary time, the geodesic itself is not obtained by imposing a global constant-time slice in the rotating coordinates.

## 2.2 Bilson’s static geodesic inversions

Bilson’s first paper treats static spherically symmetric asymptotically AdS metrics and uses two kinds of boundary information [8]. Boundary correlator singularities detect boundary-to-boundary null geodesics, while entanglement entropy in AdS<sub>3</sub> gives lengths of spacelike geodesics. Consider first the one-function global metric

$$ds^2 = -f(r)dt^2 + \frac{dr^2}{f(r)} + r^2 d\Omega_n^2. \quad (5)$$

For a null geodesic in this background, spherical symmetry allows us to restrict the motion to a great circle with angular coordinate  $\phi$ . The Killing symmetries  $\partial_t$  and  $\partial_\phi$  give two conserved quantities,

$$E = -p_t = f(r)\dot{t}, \quad J = p_\phi = r^2\dot{\phi}, \quad (6)$$

where the dot denotes differentiation with respect to an affine parameter. These are the energy and angular momentum of the probe null geodesic, not parameters of the background geometry. Bilson labels the geodesics by the ratio

$$\alpha = \frac{E}{J}, \quad (7)$$

equivalently the inverse impact parameter. The null condition means that the tangent vector of the geodesic is lightlike,  $g_{\mu\nu}\dot{x}^\mu\dot{x}^\nu = 0$ . Restricting the motion to a great circle,  $d\Omega_n^2 = d\phi^2$ , this gives

$$-f(r)\dot{t}^2 + \frac{\dot{r}^2}{f(r)} + r^2\dot{\phi}^2 = 0. \quad (8)$$

Using the conserved quantities, one obtains the radial first integral

$$\dot{r}^2 = E^2 - \frac{f(r)J^2}{r^2} = J^2 \left( \alpha^2 - \frac{f(r)}{r^2} \right), \quad \alpha = \frac{E}{J}. \quad (9)$$

The turning point  $r_{\text{min}}$  is the point at which the radial velocity vanishes. Hence, the turning point is fixed by

$$\alpha^2 = \frac{f(r_{\text{min}})}{r_{\text{min}}^2}. \quad (10)$$

The corresponding boundary time and angular separations are

$$\Delta t(\alpha) = 2 \int dt = 2 \int \frac{\dot{t}}{\dot{r}} dr = 2 \int_{r_{\text{min}}(\alpha)}^{\infty} \frac{\alpha dr}{f(r)\sqrt{\alpha^2 - f(r)/r^2}}, \quad (11)$$

$$\Delta\phi(\alpha) = 2 \int d\phi = 2 \int \frac{\dot{\phi}}{\dot{r}} dr = 2 \int_{r_{\min}(\alpha)}^{\infty} \frac{dr}{r^2 \sqrt{\alpha^2 - f(r)/r^2}}, \quad (12)$$

where the geodesic goes from the boundary to the turning point  $r_{\min}$  and returns to the boundary, so the boundary time and angular separations are twice the integrals over one radial branch. These two functions are not independent. Their endpoint variation gives

$$\frac{d}{d\alpha} [\alpha \Delta t(\alpha)] = \frac{d}{d\alpha} \Delta\phi(\alpha). \quad (13)$$

Thus one boundary function determines one radial metric function. Setting

$$V(r) = \frac{f(r)}{r^2} \quad (14)$$

and changing variables from  $r$  to  $V$ , Bilson rewrites the angular separation as a Volterra–Abel equation,

$$\Delta\phi(\sqrt{V_{\max}}) = \int_1^{V_{\max}} \frac{p(V) dV}{\sqrt{V_{\max} - V}}, \quad p(V) = -2 \frac{dr}{dV} \frac{1}{r(V)^2}. \quad (15)$$

The inversion of (15) gives  $p(V)$  and hence  $r(V)$ , after which  $f(r) = r^2 V(r)$ . The essential assumptions are that the turning-point map is monotone on the region being reconstructed and that the geometry does not hide part of the exterior behind a local maximum of the effective potential. This is the first lesson we import: inverse formulas reconstruct only the radial region swept out by the chosen geodesic family.

Bilson’s static reconstruction illustrates why the amount of boundary information matters. For a two-function static metric, equal-time spacelike geodesic lengths, or equivalently entanglement entropy in AdS<sub>3</sub>, determine only the spatial radial metric on the time-reflection slice. To recover the redshift function as well, Bilson supplements these lengths with a second boundary observable: the endpoint separations of boundary-to-boundary null geodesics, read from singularities of boundary correlators. We consider a static metric with two independent radial functions,

$$ds^2 = -f(r)dt^2 + \frac{dr^2}{h(r)} + r^2 d\Omega_n^2. \quad (16)$$

We separate the redshift function from the angular scale by writing

$$V(r) = \frac{f(r)}{r^2}. \quad (17)$$

The null condition gives the radial first integral

$$\dot{r}^2 = \frac{h(r)J^2}{r^2 V(r)} (\alpha^2 - V(r)), \quad (18)$$

so that the angular endpoint separation is

$$\Delta\phi(\alpha) = 2 \int_{r_{\min}(\alpha)}^{\rho_0} \frac{\sqrt{V(r)} dr}{r \sqrt{h(r)} \sqrt{\alpha^2 - V(r)}}, \quad (19)$$

where the turning point is determined by  $V(r_{\min}) = \alpha^2$ . Equation (19) shows why the null data alone are no longer sufficient. The measured function  $\Delta\phi(\alpha)$  does not separately determine  $V(r)$  and  $h(r)$ . After changing variables from  $r$  to  $y = V(r)$ , it determines only the combination of the metric functions as

$$\mathcal{I}_1(V(r)) \equiv -\frac{1}{rV'(r)} \sqrt{\frac{V(r)}{h(r)}}. \quad (20)$$

Here the sign follows the convention that  $V(r)$  decreases toward the boundary. Assuming that  $V(r)$  is monotonic on the radial interval probed by the geodesics,  $\Delta\phi(\alpha)$  is an Abel transform of this one-variable function. Using (19) and (20), we can express  $\mathcal{I}_1(y)$  as inversion of  $\Delta\phi(\alpha)$ ,

$$\mathcal{I}_1(y) = -\frac{1}{\pi} \frac{d}{dy} \int_1^{\sqrt{y}} \frac{\alpha \Delta\phi(\alpha) d\alpha}{\sqrt{y - \alpha^2}}. \quad (21)$$

Thus  $\mathcal{I}_1(y)$  is known directly from the null-geodesic endpoint data. It is a function of one variable  $y$ , later evaluated at  $y = V(r)$ ; it is not a functional of the unknown profile  $V(r)$ .

The missing information is supplied by spacelike geodesic lengths. On a static equal-time slice, a spacelike geodesic does not probe the redshift function  $f(r)$ ; it probes only the spatial radial metric  $h(r)$ . If  $J$  denotes the conserved angular momentum of the spacelike geodesic, then for unit-speed normalization the turning point is  $r = J$ , and the proper length is

$$L(J) = 2 \int_J^{\rho_0} \frac{r dr}{\sqrt{h(r)(r^2 - J^2)}}. \quad (22)$$

This is again an Abel transform, now of  $1/\sqrt{h(r)}$ . Inverting it gives

$$\frac{1}{\sqrt{h(r)}} = \frac{1}{r\pi} \frac{d}{dr} \int_{\rho_0}^r \frac{JL(J) dJ}{\sqrt{J^2 - r^2}}. \quad (23)$$

Therefore the spacelike geodesic-length data determine  $h(r)$ .

Once  $h(r)$  is known, the null-geodesic data determine  $V(r) = f(r)/r^2$ . Indeed, (20) becomes a first-order equation for  $V(r)$ ,

$$V'(r) + \frac{1}{r\mathcal{I}_1(V(r))} \sqrt{\frac{V(r)}{h(r)}} = 0, \quad (24)$$

to be solved with the asymptotically AdS boundary condition for  $V(r)$ . Thus the logic is not that  $h(r)$  alone determines  $f(r)$ . Rather,

spacelike lengths determine  $h(r)$ ,      null angular separations determine  $\mathcal{I}_1(y)$ ,

and together these give  $V(r) = f(r)/r^2$  through (24).

Equations (23) and (24) give the second lesson of Bilson's construction. When the static metric contains two independent functions, a single one-parameter family of boundary probes does not separate them. Bilson achieves the separation by combining spacelike geodesic lengths with null-geodesic endpoint data. In the covariant HRT problem studied below, the required independence is supplied differently: a two-variable interval entropy carries two endpoint momenta, or equivalently two conserved HRT charges, and their variation over the interval family provides the additional structure needed to reconstruct the stationary radial block.

### 2.3 Bilson's strip inversion and the equal-time obstruction

Bilson's second paper studies static planar metrics of the form [9]

$$ds^2 = R^2 \frac{-h(z)^2 dt^2 + f(z)^2 dz^2 + \sum_{i=1}^d dx_i^2}{z^2}, \quad (25)$$

and reconstructs the radial function seen by static strip minimal surfaces. For a straight belt

$$A_S = \{x_1 = x \in [-\ell/2, \ell/2], x_2, \dots, x_m \in \mathbb{R}\}, \quad (26)$$

the embedding  $z = z(x)$  gives the induced area functional

$$A_N(\ell) = R^m L^{m-1} \int_{-\ell/2}^{\ell/2} \frac{\sqrt{[z'(x)f(z)]^2 + 1}}{z^m} dx. \quad (27)$$

The  $x$ -translation Hamiltonian is conserved, and at the turning point  $z = z_*$  one obtains

$$\frac{dz}{dx} = \frac{\sqrt{z_*^{2m} - z^{2m}}}{z^m f(z)}, \quad (28)$$

so the strip width is

$$\ell(z_*) = 2 \int_0^{z_*} \frac{z^m f(z) dz}{\sqrt{z_*^{2m} - z^{2m}}}. \quad (29)$$

The renormalized area is equivalently written as

$$A_\gamma(z_*) = 2R^m L^{m-1} \int_a^{z_*} \frac{z_*^m f(z) dz}{z^m \sqrt{z_*^{2m} - z^{2m}}}. \quad (30)$$

The turning point coordinate  $z_*$  is determined directly from the entropy derivative,

$$\frac{dS_A}{d\ell} = \frac{R^d L^{d-1}}{2G_N^{(d+2)} z_*^d}. \quad (31)$$

Thus boundary data determine the turning-point coordinate before the Abel inversion is performed. Writing  $g(z) = z^{2d}$  and reducing (30) to a generalized Abel equation gives

$$f(z) = \frac{dz^d}{\pi R^d L^{d-1}} \frac{d}{dz} \int_a^z \frac{A_\gamma(z_*) z_*^{d-1} dz_*}{\sqrt{z^{2d} - z_*^{2d}}}. \quad (32)$$

This is the clean planar equal-time reference formula. Related rule-based reconstructions from equal-time entanglement data, including black-hole examples and matter-sector reconstruction after imposing a gravitational ansatz, were recently developed in [10].

However, (25) also shows the limitation. Static strip areas do not depend on the time component  $h(z)$ , because the surface lies on a constant-time slice. More generally, on a three-dimensional static slice

$$ds_{\text{slice}}^2 = \frac{1}{z^2} (A_z(z) dz^2 + h_x(z) dx^2), \quad (33)$$

there is only one equal-time interval function, whereas the slice contains two radial functions. With

$$u(z) = \frac{z}{\sqrt{h_x(z)}}, \quad (34)$$

Abel kernels involve the combination

$$\frac{\sqrt{A_z(z)}}{zu'(z)}, \quad (35)$$

rather than  $A_z(z)$  and  $h_x(z)$  separately. Hence equal-time data alone cannot disentangle the two functions without assuming that  $h(z) = 1$ . This is the precise static obstruction that the covariant construction removes.

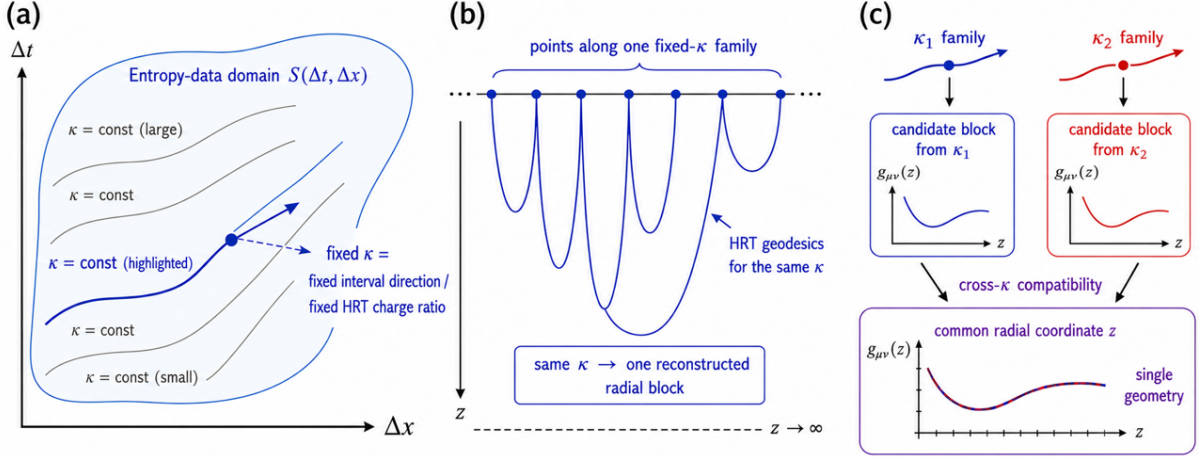


Figure 1: Schematic diagram of geometric role of fixed- $\kappa$  families in the covariant inverse problem. Panel (a) shows the two-variable interval data  $S_{\text{ren}}(\Delta t, \Delta x)$  organized by the Hamilton–Jacobi charge ratio  $\kappa = E/J$ , with  $E = -\partial_{\Delta t} L_{\text{ren}}$  and  $J = \partial_{\Delta x} L_{\text{ren}}$ . Panel (b) shows the corresponding bulk interpretation: at fixed  $\kappa$ , varying the inverse spatial momentum  $u_* = 1/J$  varies the turning point of the HRT curve and gives a one-parameter family suitable for Abel inversion. Panel (c) illustrates the cross- $\kappa$  compatibility requirement. Each fixed- $\kappa$  family gives a candidate radial block, and a single stationary homogeneous geometry exists only when these candidates agree as functions of one common radial coordinate  $z$ .

## 2.4 From static probes to covariant HRT

The HRT prescription provides the missing structure because a spacelike boundary interval in a Lorentzian conformal field theory (CFT) is labelled by two separations. In a stationary homogeneous three-dimensional bulk, the corresponding geodesic has two conserved momenta. The endpoint variation of the renormalized length gives

$$E = -\partial_{\Delta t} L_{\text{ren}}, \quad J = \partial_{\Delta x} L_{\text{ren}}, \quad \kappa = \frac{E}{J}, \quad u_* = \frac{1}{J}. \quad (36)$$

The variable  $u_*$  is the turning-point parameter, and  $\kappa$  labels the orientation of the geodesic in the boundary Lorentzian plane. More precisely, the pair of conserved charges  $(E, J)$  contains both an overall scale and a direction. The scale, equivalently  $J^{-1}$  on a fixed orientation branch, controls how deeply the HRT curve penetrates into the bulk, while the ratio  $\kappa = \frac{E}{J}$  is the projective direction of the charge vector and controls the time tilt of the curve. Thus a fixed- $\kappa$  family is not an arbitrary slice through the  $(\Delta t, \Delta x)$  plane. It is the family of HRT curves with fixed charge direction and varying turning point. This organization is summarized in Fig. 1. In the static equal-time problem,  $\kappa = 0$  is the only fixed- $\kappa$  family used. Allowing  $\kappa \neq 0$  creates the second direction in the inverse problem.

Rotating BTZ already requires this covariant viewpoint. The rotating BTZ metric may be written as

$$ds^2 = -\frac{(r^2 - r_+^2)(r^2 - r_-^2)}{r^2} dt^2 + \frac{r^2 dr^2}{(r^2 - r_+^2)(r^2 - r_-^2)} + r^2 \left( dx + \frac{r_+ r_-}{r^2} dt \right)^2. \quad (37)$$

HRT maps this geometry locally to Poincare AdS<sub>3</sub> and obtains the interval entropy

$$S_A = \frac{c}{6} \log \left[ \frac{\beta_+ \beta_-}{\pi^2 \epsilon^2} \sinh \left( \frac{\pi \Delta x^+}{\beta_+} \right) \sinh \left( \frac{\pi \Delta x^-}{\beta_-} \right) \right], \quad \beta_{\pm} = \frac{2\pi \ell}{r_{\pm} \pm r_-}, \quad (38)$$

where  $\Delta x^{\pm} = \Delta x \pm \Delta t$ . The equality with the left-right asymmetric conformal-field-theory calculation is part of the evidence for the covariant prescription. More importantly, rotating

BTZ is stationary but non-static: the Killing field is not hypersurface orthogonal. The extremal curve is therefore not obtained by first choosing a constant-time bulk slice. Thus, in a stationary non-static background, the HRT extremal problem is the appropriate variational problem.

For a general stationary homogeneous metric, Section 3 will show that the data in (36) produce three Abel kernels. Their cross-family compatibility reconstructs the three inverse-block functions of the metric. The result reduces to Bilson in the one-function static limit, but it also explains why the equal-time restriction fails once  $h_x(z)$  or a stationary shift is allowed.

We restrict to a fixed sector in which the construction can be made explicit. The analysis assumes a stationary homogeneous three-dimensional metric in a fixed radial gauge and asks whether the covariant interval entropy alone reconstructs the radial metric block. The answer is constructive: the Abel kernels recover the metric, while the admissibility conditions tell us when a candidate entropy function can have such a geometric origin.

### 3 Inversion formula from covariant holographic entanglement entropy

The preceding section reviewed why the static inversion requires the correct number of independent probes. In the stationary problem the additional data are not supplied by a separate observable. They are already present in the covariant interval entropy: its endpoint variation gives two conserved charges rather than one. The aim of this section is to turn the two-charge structure of Hubeny–Rangamani–Takayanagi (HRT) geodesics into a radial reconstruction of the metric block.

#### 3.1 Stationary metric class and Hamilton–Jacobi variables

The natural geometric starting point is not the special Bañados–Teitelboim–Zanelli (BTZ) form, but the stationary homogeneous radial-gauge metric

$$ds^2 = \frac{1}{z^2} \left[ G(z) dz^2 + \gamma_{ab}(z) dx^a dx^b \right], \quad x^a = (t, x). \quad (39)$$

The residual freedom  $z \mapsto \tilde{z}(z)$  means that a radial gauge must be fixed before one can speak of reconstructing the radial metric functions uniquely. The boundary interval entropy determines the geometry only up to this radial coordinate choice.

For any Lorentzian two-dimensional block with  $\gamma_{xx} > 0$ , one may complete the square as

$$\gamma_{ab} dx^a dx^b = -N(z)^2 dt^2 + H(z) (dx + V(z) dt)^2. \quad (40)$$

This is the Arnowitt–Deser–Misner (ADM) form of the  $(t, x)$  block. It is not a loss of generality within the homogeneous stationary sector; it is a parametrization of a two-by-two Lorentzian matrix.

A convenient black-brane radial gauge is

$$N(z)^2 = f(z), \quad H(z) = h(z), \quad V(z) = v(z), \quad G(z) = \frac{1}{f(z)}. \quad (41)$$

Then

$$ds^2 = \frac{1}{z^2} \left[ -f(z) dt^2 + \frac{dz^2}{f(z)} + h(z) (dx + v(z) dt)^2 \right]. \quad (42)$$

This gauge is adapted to BTZ and black-brane examples, but the derivation below should be read as a fixed-radial-gauge statement. In Fefferman–Graham gauge, for example, one would set  $G(z) = 1$  instead; the ratio formulae for the boundary block are unchanged, while the equation that reconstructs the radial coordinate is modified by the corresponding  $G(z)$ .

With the convention (42), define

$$A(z) = \frac{1}{f(z)}, \quad B(z) = \frac{v(z)}{f(z)}, \quad C(z) = \frac{1}{h(z)} - \frac{v(z)^2}{f(z)}. \quad (43)$$

These are not arbitrary variables; they are the inverse metric combinations that enter the geodesic Hamiltonian. The inverse of the  $(t, x)$  block is

$$\gamma^{tt} = -A, \quad \gamma^{tx} = B, \quad \gamma^{xx} = C. \quad (44)$$

The original variables are recovered algebraically from  $A, B, C$ :

$$f = \frac{1}{A}, \quad v = \frac{B}{A}, \quad h = \frac{1}{C + B^2/A}. \quad (45)$$

Thus the inverse problem can be stated as the reconstruction of  $A, B, C$  in the chosen radial gauge<sup>2</sup>.

Let  $L(\Delta t, \Delta x) = 4G_N S_{\text{ren}}(\Delta t, \Delta x)$  be the renormalized on-shell HRT length for a spacelike boundary interval. The endpoint variation of the on-shell action gives the canonical momenta at the boundary. With the symmetric convention that the interval endpoints are separated by  $(\Delta t, \Delta x)$ , we write

$$E = -\partial_{\Delta t} L, \quad J = \partial_{\Delta x} L. \quad (46)$$

The ratio

$$\kappa = \frac{E}{J} = -\frac{\partial_{\Delta t} S_{\text{ren}}}{\partial_{\Delta x} S_{\text{ren}}} \quad (47)$$

and the inverse spatial momentum

$$u_* = \frac{1}{J} = \frac{1}{\partial_{\Delta x} L} \quad (48)$$

are therefore determined by the interval dependence of the holographic entanglement entropy. A curve of fixed  $\kappa$  in the interval plane will be called a fixed- $\kappa$  family. This terminology refers only to the organization of the boundary interval data; it does not impose an additional restriction on the bulk metric.

In what follows we restrict attention to a range of spacelike intervals for which the same HRT saddle varies smoothly as  $(\Delta t, \Delta x)$  is changed. In this range  $L$  is a smooth function of the interval endpoints, rather than the lower envelope of several competing extremal lengths. Equivalently, on the interval domain under consideration the chosen saddle  $L_\alpha$  is  $C^3$  and separated from the other saddles,  $L_\beta - L_\alpha > 0$  for all competing  $\beta \neq \alpha$ . We also assume that the interval data can be used to parametrize the corresponding geodesics by  $(\kappa, u_*)$ , namely

$$J \neq 0, \quad \det \frac{\partial(\kappa, u_*)}{\partial(\Delta t, \Delta x)} \neq 0. \quad (49)$$

At points where  $J = 0$ , the ratio  $E/J$  is singular. At caustics, turning-point degeneracies, or HRT phase transitions, the map from boundary intervals to  $(\kappa, u_*)$  no longer describes one smooth family of geodesics. The reconstruction below therefore applies only to the radial region reached by this chosen HRT family. Large intervals on compact boundaries, entanglement plateaux, black-hole homology transitions, and multiboundary wormhole phases are not covered by a single application of the formula; in such cases the competing HRT saddles must first be separated.

---

<sup>2</sup>We note that sign convention is  $dx + vdt$  throughout. Replacing it by  $dx - vdt$  sends  $B \rightarrow -B$  and changes the sign of every term linear in  $B$ . No physical result depends on this convention, but the convention must not be mixed within a derivation.

### 3.2 Characteristic Abel inversion and metric reconstruction

Parametrize the spacelike HRT geodesic by proper length  $s$ , so that

$$g_{\mu\nu}\dot{X}^\mu\dot{X}^\nu = 1, \quad (50)$$

where dot implies  $\frac{d}{ds}$ . From (42), the conserved energy and spatial momentum are

$$E = \frac{(f - hv^2)\dot{t} - hv\dot{x}}{z^2}, \quad J = \frac{hv\dot{t} + h\dot{x}}{z^2}. \quad (51)$$

Solving for the velocities gives

$$\dot{t} = z^2 \frac{E + vJ}{f}, \quad \dot{x} = z^2 \frac{J}{h} - z^2 v \frac{E + vJ}{f}. \quad (52)$$

We choose the affine parameter  $s$  along the spacelike HRT geodesic to be proper length, so that  $g_{\mu\nu}\dot{X}^\mu\dot{X}^\nu = 1$ . Using the conserved charges  $E$  and  $J$ , this unit-speed condition gives

$$\dot{z}^2 = z^2 f(z) \left[ 1 - z^2 \left( \frac{J^2}{h(z)} - \frac{(E + v(z)J)^2}{f(z)} \right) \right]. \quad (53)$$

Introduce

$$\kappa = \frac{E}{J}, \quad \Psi_\kappa(z) = C(z) - 2\kappa B(z) - \kappa^2 A(z). \quad (54)$$

Then

$$\frac{J^2}{h} - \frac{(E + vJ)^2}{f} = J^2 \Psi_\kappa(z), \quad (55)$$

and the radial equation becomes

$$\dot{z}^2 = z^2 f(z) [1 - J^2 z^2 \Psi_\kappa(z)]. \quad (56)$$

The turning point  $z = z_*$  is the point where the geodesic reverses its radial motion, hence

$$\dot{z}(z_*) = 0. \quad (57)$$

Assuming  $z_*$  is outside any zero of  $f$  on the branch considered, (56) gives

$$1 - J^2 z_*^2 \Psi_\kappa(z_*) = 0. \quad (58)$$

Define the characteristic radial variable

$$u_\kappa(z) = z \sqrt{\Psi_\kappa(z)}. \quad (59)$$

Then (58) is simply

$$J^2 u_\kappa(z_*)^2 = 1. \quad (60)$$

For the orientation  $J > 0$ , this gives

$$u_* = u_\kappa(z_*) = \frac{1}{J}. \quad (61)$$

For  $J < 0$ , one uses  $u_* = 1/|J|$  with the corresponding orientation convention. In the following we work on a branch with  $J > 0$ .

Using (52) and (56), one obtains

$$\frac{dt}{dz} = \frac{Jz\sqrt{A(z)}(\kappa A(z) + B(z))}{\sqrt{1 - J^2 z^2 \Psi_\kappa(z)}}, \quad (62)$$

and

$$\frac{dx}{dz} = \frac{Jz\sqrt{A(z)}(C(z) - \kappa B(z))}{\sqrt{1 - J^2 z^2 \Psi_\kappa(z)}}. \quad (63)$$

For a symmetric geodesic, the boundary separations are twice the integral from the boundary to the turning point:

$$\frac{\Delta t_\kappa}{2} = J \int_0^{z^*} \frac{z\sqrt{A}(\kappa A + B)}{\sqrt{1 - J^2 u_\kappa(z)^2}} dz, \quad (64)$$

$$\frac{\Delta x_\kappa}{2} = J \int_0^{z^*} \frac{z\sqrt{A}(C - \kappa B)}{\sqrt{1 - J^2 u_\kappa(z)^2}} dz. \quad (65)$$

Similarly, since  $\dot{z} = dz/ds$ , changing variables in the proper-length integral  $L = \int ds$  gives  $ds = dz/|\dot{z}|$  on each radial branch. The regulated geodesic length is therefore

$$L_\kappa(\epsilon) = 2 \int_\epsilon^{z^*} \frac{dz}{|\dot{z}|} = 2 \int_\epsilon^{z^*} \frac{\sqrt{A(z)}}{z\sqrt{1 - J^2 u_\kappa(z)^2}} dz. \quad (66)$$

As usual for an asymptotically anti-de Sitter (AdS) geodesic, this expression contains the universal endpoint divergence. We define the renormalized length by

$$L_{\kappa,\text{ren}} = \lim_{\epsilon \rightarrow 0} [L_\kappa(\epsilon) + L_{\text{ct}}(\epsilon)], \quad (67)$$

where  $L_{\text{ct}}$  subtracts only the standard cutoff-dependent boundary divergence. The subtraction affects only the usual UV divergence; it does not change the Abel kernel in the interior. The Abel inversion is formulated for the renormalized length. The bare geodesic length contains the usual asymptotically AdS endpoint divergence, but this divergence is local at the boundary and is removed by  $L_{\text{ct}}(\epsilon)$ . Since the counterterm is independent of the bulk turning point and of the interior radial kernel, it does not affect the Abel transform. It only fixes the finite normalization of the holographic entanglement entropy input.

Assume on the branch under consideration that

$$u'_\kappa(z) \neq 0, \quad (68)$$

so that  $z$  can be used as a function of  $u$  at fixed  $\kappa$ . Since  $J = 1/u_*$ , the denominator becomes

$$\sqrt{1 - J^2 u^2} = \frac{\sqrt{u_*^2 - u^2}}{u_*}. \quad (69)$$

Changing variables from  $z$  to  $u$  gives

$$L_\kappa(u_*) = 2u_* \int_0^{u_*} \frac{F_\kappa(u)}{\sqrt{u_*^2 - u^2}} du, \quad (70)$$

where

$$F_\kappa(u) = \left. \frac{\sqrt{A(z)}}{z u'_\kappa(z)} \right|_{z=z_\kappa(u)}. \quad (71)$$

The endpoint integrals become

$$\frac{\Delta t_\kappa(u_*)}{2} = \int_0^{u_*} \frac{T_\kappa(u)}{\sqrt{u_*^2 - u^2}} du, \quad (72)$$

$$\frac{\Delta x_\kappa(u_*)}{2} = \int_0^{u_*} \frac{X_\kappa(u)}{\sqrt{u_*^2 - u^2}} du, \quad (73)$$

with

$$T_\kappa(u) = \frac{z\sqrt{A(z)}(\kappa A(z) + B(z))}{u'_\kappa(z)} \Big|_{z=z_\kappa(u)}, \quad (74)$$

and

$$X_\kappa(u) = \frac{z\sqrt{A(z)}(C(z) - \kappa B(z))}{u'_\kappa(z)} \Big|_{z=z_\kappa(u)}. \quad (75)$$

These equations explain the endpoint kernels used in the inversion. They are not additional assumptions; they follow from  $dt/dz$ ,  $dx/dz$ , the turning-point relation  $J = 1/u_*$ , and the change of variables  $z \mapsto u_\kappa(z)$ .

The inverse Abel formulae are

$$F_\kappa(u) = \frac{1}{\pi} \frac{d}{du} \int_0^u \frac{2y \mathcal{L}_\kappa(y)}{\sqrt{u^2 - y^2}} dy, \quad \mathcal{L}_\kappa(u) = \frac{L_\kappa(u)}{2u}, \quad (76)$$

$$T_\kappa(u) = \frac{1}{\pi} \frac{d}{du} \int_0^u \frac{y \Delta t_\kappa(y)}{\sqrt{u^2 - y^2}} dy, \quad (77)$$

$$X_\kappa(u) = \frac{1}{\pi} \frac{d}{du} \int_0^u \frac{y \Delta x_\kappa(y)}{\sqrt{u^2 - y^2}} dy. \quad (78)$$

Define the ratio functions

$$R_t(\kappa, u) = \frac{T_\kappa(u)}{F_\kappa(u)}, \quad R_x(\kappa, u) = \frac{X_\kappa(u)}{F_\kappa(u)}. \quad (79)$$

Using (71), (74), and (75), one obtains the pointwise identities

$$R_t = z^2(\kappa A + B), \quad (80)$$

$$R_x = z^2(C - \kappa B), \quad (81)$$

and therefore

$$R_x - \kappa R_t = z^2 \Psi_\kappa(z) = u^2. \quad (82)$$

A technical distinction is that  $F_\kappa, T_\kappa, X_\kappa$  are functions of  $u$ , while the metric functions are functions of the common radial coordinate  $z$ . The derivative at fixed  $z$  is not the same as the derivative at fixed  $u$ . From

$$u^2 = z^2 \Psi_\kappa(z), \quad (83)$$

we find

$$(\partial_\kappa u^2)_z = z^2 \partial_\kappa \Psi_\kappa = -2z^2(\kappa A + B) = -2R_t. \quad (84)$$

Hence

$$(\partial_\kappa u)_z = -\frac{R_t}{u}. \quad (85)$$

Using the chain rule, the derivative at fixed radial position is therefore

$$D_\kappa := (\partial_\kappa)_z = \partial_\kappa - \frac{R_t}{u} \partial_u. \quad (86)$$

Applying this operator to (80) gives

$$D_\kappa R_t = z^2 A. \quad (87)$$

Similarly, applying it to (81) gives

$$D_\kappa R_x = -z^2 B. \quad (88)$$

These two identities are the ingredients absent from the static equal-time Abel inversion.

In the gauge (42),  $G = A$ . Equation (71) reads

$$F_\kappa = \frac{\sqrt{A}}{z u'_\kappa(z)}. \quad (89)$$

Using (87),

$$\sqrt{A} = \frac{\sqrt{D_\kappa R_t}}{z}. \quad (90)$$

Since  $\partial_u z = 1/u'_\kappa(z)$ , we obtain

$$\partial_u z = \frac{F_\kappa z^2}{\sqrt{D_\kappa R_t}}, \quad (91)$$

or equivalently

$$\partial_u \left( \frac{1}{z} \right) = - \frac{F_\kappa(u)}{\sqrt{D_\kappa R_t(\kappa, u)}}. \quad (92)$$

The equation for  $z(\kappa, u)$  must be supplemented by its near-boundary behaviour. In the gauge (42), standard asymptotically AdS boundary conditions in a non-rotating boundary frame are

$$f(z) \rightarrow 1, \quad h(z) \rightarrow 1, \quad v(z) \rightarrow 0 \quad (z \rightarrow 0). \quad (93)$$

Equivalently,

$$A \rightarrow 1, \quad B \rightarrow 0, \quad C \rightarrow 1. \quad (94)$$

Since  $u^2 = z^2 \Psi_\kappa(z)$ ,  $\Psi_\kappa = C - 2\kappa B - \kappa^2 A$ , we obtain near the boundary

$$u^2 \sim z^2(1 - \kappa^2), \quad u \sim z\sqrt{1 - \kappa^2}. \quad (95)$$

Thus

$$\frac{1}{z} \sim \frac{\sqrt{1 - \kappa^2}}{u} \quad (u \rightarrow 0). \quad (96)$$

This leading term is the universal asymptotically AdS boundary behavior. Correspondingly,

$$\frac{F_\kappa(u)}{\sqrt{D_\kappa R_t(\kappa, u)}} \sim \frac{\sqrt{1 - \kappa^2}}{u^2} \quad (97)$$

near  $u = 0$ . The integral solution (92) is therefore written after subtracting this universal endpoint divergence:

$$\frac{1}{z(\kappa, u)} = \frac{\sqrt{1 - \kappa^2}}{u} - \int_0^u \left[ \frac{F_\kappa(s)}{\sqrt{D_\kappa R_t(\kappa, s)}} - \frac{\sqrt{1 - \kappa^2}}{s^2} \right] ds.$$

The integrand in the square brackets is finite for geometries with the standard asymptotically AdS expansion.

Once  $z(\kappa, u)$  has been determined, (87), (80), and (81) give

$$A = \frac{D_\kappa R_t}{z^2}, \quad (98)$$

$$B = \frac{R_t - \kappa D_\kappa R_t}{z^2}, \quad (99)$$

$$C = \frac{R_x + \kappa R_t - \kappa^2 D_\kappa R_t}{z^2}. \quad (100)$$

Finally,

$$f = \frac{1}{A}, \quad v = \frac{B}{A}, \quad h = \frac{1}{C + B^2/A}. \quad (101)$$

Thus the covariant HRT data determine the stationary radial metric block on the portion of the bulk reached by the chosen smooth geodesic family. If the physical entropy is instead a lower envelope of several extremal saddles, the construction applies only after one resolves the smooth geodesic families separately.

### 3.3 Causal readout of the reconstructed metric

The formula above reconstructs the stationary radial block, but the same block also determines the local causal structure projected to the stationary  $(t, x)$ -plane. This is a structural consequence of the inverse map, not an additional assumption. At fixed radial position, a projected null direction  $\lambda = dx/dt$  obeys

$$g_{tt} + 2\lambda g_{tx} + \lambda^2 g_{xx} = 0. \quad (102)$$

For the metric (42), this is

$$-f(z) + h(z)(\lambda + v(z))^2 = 0. \quad (103)$$

Hence the two projected null directions are

$$\lambda_{\pm}(z) = -v(z) \pm \sqrt{\frac{f(z)}{h(z)}}. \quad (104)$$

In terms of the reconstructed inverse block variables,

$$A = \frac{1}{f}, \quad B = \frac{v}{f}, \quad C = \frac{1}{h} - \frac{v^2}{f}, \quad (105)$$

this becomes

$$\lambda_{\pm}(z) = \frac{-B(z) \pm \sqrt{B(z)^2 + A(z)C(z)}}{A(z)}. \quad (106)$$

Thus the projected light cone is fixed algebraically once  $A, B, C$  have been reconstructed. Conversely,

$$v(z) = -\frac{\lambda_+(z) + \lambda_-(z)}{2}, \quad \frac{f(z)}{h(z)} = \frac{(\lambda_+(z) - \lambda_-(z))^2}{4}. \quad (107)$$

The midpoint of the two roots is the local frame-dragging shift, while their separation is the opening of the projected cone.

If the branch reaches a stationary horizon at  $z = z_h$ , with  $f(z_h) = 0$  and finite  $h(z_h)$ , the two roots coalesce:

$$\lambda_+(z_h) = \lambda_-(z_h) = -v(z_h) = -\Omega_H. \quad (108)$$

This is the projected horizon generator. A stationary-limit surface is located by the vanishing norm of  $\partial_t$ ,

$$g_{tt} = z^{-2}(-f + hv^2) = 0. \quad (109)$$

Using  $C = (f - hv^2)/(fh)$ , this is equivalent to

$$C(z) = 0 \quad \iff \quad \lambda_+(z)\lambda_-(z) = 0. \quad (110)$$

Thus, one projected null direction has  $dx/dt = 0$  precisely when the stationary Killing direction becomes null. In this sense, the covariant entropy data, after inversion, determine not only radial distances but also frame dragging, the horizon generator, and the stationary-limit surface.

For the rotating BTZ block reconstructed below,

$$f(z) = (1 - z^2)(1 - \Omega^2 z^2), \quad h(z) = 1, \quad v(z) = \Omega z^2, \quad (111)$$

so the general formula gives

$$\lambda_{\pm}(z) = -\Omega z^2 \pm \sqrt{(1 - z^2)(1 - \Omega^2 z^2)}. \quad (112)$$

These roots approach  $\pm 1$  near the boundary, coalesce at the horizon with common value  $-\Omega$ , and one root crosses zero at the stationary-limit surface.

Hence, we can conclude that considering a stationary homogeneous three-dimensional metric in the gauge (42) and supposing that the holographic entanglement entropy is evaluated on a range of spacelike boundary intervals for which the same HRT saddle varies smoothly, the renormalized length

$$L = 4G_N S_{\text{ren}}$$

has well-defined endpoint derivatives and Abel kernels. Assume moreover that the change of variables from interval data to  $(\kappa, u_*)$  is non-degenerate, that  $u'_\kappa(z) \neq 0$  on the radial range reached by this family of geodesics, and that  $D_\kappa R_t = z^2 A > 0$  so that the reconstructed radial metric coefficient is real and positive. Then the holographic entanglement entropy determines  $f(z), h(z), v(z)$  on that radial range through (76)–(101).

Conversely, suppose that a candidate holographic entanglement entropy produces smooth Abel kernels satisfying the admissibility conditions of Section 3.4, together with the same positivity, asymptotic AdS, and smooth-saddle assumptions. Then (76)–(101) construct a local stationary homogeneous radial metric block whose Abel kernels reproduce the input holographic entanglement entropy.

Bilson’s static inversion has one turning-point family, so there is no transverse characteristic direction along which different boosted intervals must agree. The covariant problem has a two-variable Hamilton–Jacobi chart, and the quantities reconstructed from different values of  $\kappa$  must glue to the same functions of one radial coordinate. The integrability equations below are exactly this cross-family compatibility condition.

The positivity condition is essential because the matching equation for  $z(\kappa, u)$  is a first-order equation whose real solution requires a positive square root. By (87) it is  $z^2 A > 0$ . In the gauge (42) this is equivalent to  $f > 0$ , hence to working outside the horizon or before the endpoint of the radial branch. The monotonicity condition on  $u_\kappa(z)$  ensures that the change of variables  $z \leftrightarrow u$  is single-valued.

### 3.4 Admissibility conditions and higher-dimensional extension

The reconstruction formula also imposes local constraints on any candidate two-variable function  $S_{\text{ren}}(\Delta t, \Delta x)$ . These constraints are the covariant analogue of the monotonicity and Abel-invertibility assumptions in Bilson’s static analysis: they are not additional physics input, but the consistency conditions required for the boundary data to come from a stationary homogeneous HRT problem.

**Condition 1.** The first condition is algebraic. The three Abel kernels  $X_\kappa, F_\kappa$ , and  $T_\kappa$  obtained from the length, time, and spatial endpoint equations must come from the same Hamiltonian system. If they come from one stationary HRT geodesic problem, the length, time, and spatial endpoint integrals must share the same radial variable  $u_\kappa(z)$  and the same square-root Hamiltonian constraint. This gives the algebraic compatibility condition

$$X_\kappa - u^2 F_\kappa - \kappa T_\kappa = 0.$$

After Abel inversion this becomes

$$R_x - \kappa R_t - u^2 = 0.$$

Indeed, for a genuine stationary metric one has

$$R_t = z^2(\kappa A + B), \quad R_x = z^2(C - \kappa B),$$

while

$$u^2 = z^2(C - 2\kappa B - \kappa^2 A).$$

Hence  $R_x - \kappa R_t = u^2$ . Applying the characteristic derivative to this identity gives the shift-readout relation

$$D_\kappa R_x + R_t - \kappa D_\kappa R_t = 0, \quad z^2 B = -D_\kappa R_x = R_t - \kappa D_\kappa R_t. \quad (113)$$

This is the point at which the covariant problem differs most sharply from the equal-time static one. The mixed component  $B = v/f$  of the stationary inverse block is not fitted separately. It is isolated by comparing the spatial endpoint response across the  $\kappa$ -family at fixed radial position:

$$B = -\frac{1}{z^2} D_\kappa R_x.$$

The stationary shift is read from the  $\kappa$ -dependence of the endpoint response.

**Condition 2.** The next condition expresses the common-geometry requirement. At this stage  $F_\kappa, T_\kappa, X_\kappa$  are reconstructed from the boundary holographic entanglement entropy. They are functions of the Abel variable  $u$  and the charge ratio  $\kappa$ . We have not yet assumed that there exists a radial coordinate  $z$  and metric functions  $A(z), B(z), C(z)$  producing them. The following conditions are precisely the conditions for such a common radial description to exist. In the forward problem the identities  $R_t = z^2(\kappa A + B)$  and  $R_x = z^2(C - \kappa B)$  are automatic. In the inverse problem they are not definitions. The quantities  $R_t$  and  $R_x$  are first obtained from the entropy kernels, and the question is whether there exists a common radial coordinate  $z$  in which they take this metric form. Thus, after comparing different  $\kappa$ 's at the same bulk radius, the dependence on  $\kappa$  must have the special linear form. Applying the fixed-radius derivative gives  $D_\kappa R_t = z^2 A$ ,  $D_\kappa R_x = -z^2 B$ . Since  $A$  and  $B$  are functions of  $z$  only, the right-hand sides have no further  $\kappa$ -dependence at fixed  $z$ . Hence

$$D_\kappa^2 R_t = 0, \quad D_\kappa^2 R_x = 0.$$

Equivalently,  $R_t$  and  $R_x$  must be at most linear in  $\kappa$  at fixed  $z$ . Failure of this condition means that the different  $\kappa$ -families cannot be combined into one stationary homogeneous radial metric block. These two equations are the local integrability test for the stationary homogeneous ansatz. They reduce the apparent two-variable freedom of  $R_t(\kappa, u)$  and  $R_x(\kappa, u)$  to three radial functions  $A, B, C$  together with the choice of radial coordinate. This is the main obstruction that has no analogue in the one-function static inversion. If a candidate entropy produces

$$D_\kappa^2 R_t \neq 0 \quad \text{or} \quad D_\kappa^2 R_x \neq 0 \quad (114)$$

within an assumed smooth branch, then the data do not come from a single stationary homogeneous three-dimensional HRT geometry in the class under consideration. It can mean that the state is time dependent or spatially inhomogeneous, that the entropy is crossing between competing HRT saddles, or that the relevant extremal surface belongs to a higher-dimensional strip problem whose transverse area density has not been separated. In each case, the boundary function may still be meaningful, but it is not the classical interval entropy of the stationary three-dimensional sector reconstructed here.

**Condition 3.** The length kernel fixes the relation between the Abel variable and the radial coordinate. Define

$$Q(\kappa, u) \equiv \frac{F_\kappa(u)}{\sqrt{D_\kappa R_t(\kappa, u)}}. \quad (115)$$

For a genuine stationary metric,

$$F_\kappa = \frac{\sqrt{A}}{z u'_\kappa(z)}, \quad D_\kappa R_t = z^2 A, \quad (116)$$

and therefore

$$Q = \frac{1}{z^2 u'_\kappa(z)} = \frac{1}{z^2} \frac{\partial z}{\partial u}. \quad (117)$$

Equivalently,

$$\partial_u \left( \frac{1}{z} \right) = -Q. \quad (118)$$

This equation reconstructs the radial coordinate along each fixed- $\kappa$  family. A stationary geometry requires the different families to share the same radial coordinate. Since  $D_\kappa$  differentiates at fixed  $z$ , this means

$$D_\kappa \left( \frac{1}{z} \right) = 0. \quad (119)$$

The two equations for  $1/z$  are compatible only if

$$D_\kappa \log Q = \partial_u \left( \frac{R_t}{u} \right). \quad (120)$$

To see this, write  $a = R_t/u$ , so that  $D_\kappa = \partial_\kappa - a\partial_u$ . Then

$$[D_\kappa, \partial_u] = (\partial_u a)\partial_u. \quad (121)$$

Applying this commutator to  $1/z$ , together with  $\partial_u(1/z) = -Q$  and  $D_\kappa(1/z) = 0$ , gives the stated condition (120). This is the Frobenius condition for a common radial coordinate. If it fails, each fixed- $\kappa$  family may define its own Abel coordinate, but the families cannot be identified as slices of one stationary radial geometry.

**Condition 4.** The remaining constraints are the usual signature and boundary conditions written in the reconstructed variables. From

$$A = \frac{D_\kappa R_t}{z^2}, \quad B = -\frac{D_\kappa R_x}{z^2}, \quad C = \frac{R_x + \kappa R_t - \kappa^2 D_\kappa R_t}{z^2}, \quad (122)$$

the exterior radial condition  $A > 0$  gives  $D_\kappa R_t > 0$ . Moreover,

$$h^{-1} = C + \frac{B^2}{A} = \frac{1}{z^2} [D_\kappa R_t (R_x + \kappa R_t - \kappa^2 D_\kappa R_t) + (D_\kappa R_x)^2], \quad (123)$$

so positivity of the spatial warp factor gives

$$D_\kappa R_t (R_x + \kappa R_t - \kappa^2 D_\kappa R_t) + (D_\kappa R_x)^2 > 0. \quad (124)$$

We shall refer to the collection

$$\begin{aligned} R_x - \kappa R_t - u^2 &= 0, & D_\kappa R_x + R_t - \kappa D_\kappa R_t &= 0, \\ D_\kappa^2 R_t &= 0, & D_\kappa^2 R_x &= 0, & D_\kappa \log Q &= \partial_u (R_t/u), \\ D_\kappa R_t &> 0, & D_\kappa R_t (R_x + \kappa R_t - \kappa^2 D_\kappa R_t) &+ (D_\kappa R_x)^2 &> 0 \end{aligned} \quad (125)$$

as the local admissibility conditions. They express the overdetermination of covariant interval entropy: a generic function of two boundary variables does not satisfy (125).

**Higher-dimensional extension.** The reconstruction theorem above is formulated for AdS<sub>3</sub>, where the HRT surface of an interval is a curve and the entropy is proportional to a geodesic length. In higher dimensions, the HRT surface has transverse volume, so the entropy is an area rather than a length. Therefore the three-dimensional formula should not be read as reconstructing a higher-dimensional metric directly. The formula applies only after the HRT area problem has been reduced, by symmetry, to an effective one-dimensional variational problem.

To make this explicit, consider a homogeneous strip which is finite in the  $x$ -direction and extended along the transverse directions  $y_a$ . On an equal-time slice write the spatial metric as

$$ds_{\text{spatial}}^2 = \frac{1}{z^2} \left[ G(z)dz^2 + H_x(z)dx^2 + \sum_{a=2}^{d-1} H_a(z)dy_a^2 \right].$$

After dividing by the coordinate volume of the transverse directions, the HRT area functional is

$$\mathcal{A}_x = \int dx W_x(z) \sqrt{H_x(z) + G(z)z'(x)^2}, \quad W_x(z) = z^{-(d-1)} \prod_{a=2}^{d-1} \sqrt{H_a(z)}. \quad (126)$$

The factor  $W_x(z)$  is absent in the AdS<sub>3</sub> interval problem. It is the transverse area density carried by the strip surface.

Equation (126) can be rewritten as the length functional of a curve in a density-dressed two-dimensional spatial metric,

$$d\bar{s}_{x,\text{spatial}}^2 = W_x(z)^2 [G(z)dz^2 + H_x(z)dx^2].$$

Thus a single strip orientation does not directly reconstruct  $G(z)$  and  $H_x(z)$ . It reconstructs the effective two-dimensional geometry seen by that strip. Equivalently, it determines the combinations

$$P_x(z) = W_x(z) \sqrt{H_x(z)}, \quad \Xi_x(P_x) = \sqrt{\frac{G(z)}{H_x(z)}} \left| \frac{dz}{dP_x} \right|. \quad (127)$$

Here  $P_x$  is the effective spatial scale seen by the  $x$ -strip, and  $\Xi_x$  is the corresponding radial factor after using  $P_x$  as the radial variable. The original metric functions are recovered only if the dressing factor  $W_x$  is known or can be separated from other region data.

In an isotropic spatial sector this separation is automatic. If all spatial warp factors are tied to one common function, then the transverse density  $W_x$  is fixed by the same function that controls the finite-width direction. One may use the common spatial volume scale  $P$  as the radial coordinate and write

$$ds_{\text{spatial}}^2 = P^{2/(d-1)} (d\vec{x}^2 + \Xi(P)^2 dP^2). \quad (128)$$

In this special case the strip entropy reduces to a closed one-function inversion problem.

In an anisotropic spatial sector, one strip orientation is not enough. For example, with two boundary spatial directions, an  $x$ -strip is extended along  $y$  and therefore contains the transverse factor associated with the  $y$ -direction, while a  $y$ -strip contains the transverse factor associated with the  $x$ -direction. The two orientations can determine the relative anisotropy, but not an independent overall radial normalization without an additional choice of radial variable. A convenient parametrization is to use

$$P = \sqrt{\gamma_x \gamma_y}$$

as the common spatial scale and write

$$\gamma_x = P \frac{\Xi_y}{\Xi_x}, \quad \gamma_y = P \frac{\Xi_x}{\Xi_y}, \quad \gamma_{PP} = P \Xi_x \Xi_y. \quad (129)$$

This parametrization makes clear what is, and is not, determined. In a bulk dimension  $D$ , the boundary has  $n = D - 2$  spatial directions. If the spatial sector is isotropic, all these directions share one warp factor, and the strip entropy closes on a one-function spatial inversion after a radial coordinate has been chosen. This remains true in any  $D$ ; the dimension changes the power with which the common warp factor enters the transverse density, but it does not introduce new independent spatial functions. By contrast, an anisotropic spatial sector contains independent warp factors  $H_i(z)$ . After one common volume scale is absorbed into the radial coordinate, there remain  $n - 1$  relative anisotropy functions. A single strip orientation only reconstructs the density-dressed two-dimensional metric seen by that strip. To recover the undressed anisotropic metric one needs strip data in enough independent orientations to separate these relative warp factors. Thus, in  $D = 4$ , where  $n = 2$ ,  $x$ - and  $y$ -oriented strips can separate the single relative anisotropy. In higher dimensions, the number of required orientations grows with the number of independent anisotropic spatial directions, not with the dimension by itself.

The same density-dressing issue persists for covariant HRT strips in stationary geometries. We now allow the reduced  $(t, z, x)$  block to be stationary rather than purely spatial, while keeping the strip finite in the  $x$ -direction and extended along the transverse directions. Thus this is still a higher-dimensional strip problem, but now the HRT surface may carry time separation and can probe a stationary shift  $v(z)$ , the analogue of frame dragging in the reduced block.

For such an  $x$ -oriented strip, the area density reduces to a three-dimensional stationary block multiplied by the same transverse density  $W_x(z)$ :

$$d\bar{s}_x^2 = W_x(z)^2 [G(z)dz^2 - N(z)^2 dt^2 + H_x(z)(dx + v_x(z)dt)^2].$$

The barred variables refer to the inverse block of this density-dressed three-dimensional metric. If  $(A_x, B_x, C_x)$  are the inverse-block variables of the undressed  $(t, x)$  stationary sector, multiplication of the reduced metric by  $W_x^2$  divides its inverse block by  $W_x^2$ :

$$\bar{A}_x = \frac{A_x}{W_x^2}, \quad \bar{B}_x = \frac{B_x}{W_x^2}, \quad \bar{C}_x = \frac{C_x}{W_x^2}. \quad (130)$$

Therefore the three-dimensional covariant inversion formulae apply directly to  $(\bar{A}_x, \bar{B}_x, \bar{C}_x)$ , not to the undressed variables  $(A_x, B_x, C_x)$ .

One quantity is nevertheless undressed already at this stage. The same factor  $W_x^2$  multiplies the  $tt$ ,  $tx$ , and  $xx$  components of the reduced stationary block. Hence it cancels in the ratio

$$\frac{\bar{B}_x}{\bar{A}_x} = \frac{B_x/W_x^2}{A_x/W_x^2} = \frac{B_x}{A_x} = v_x(z). \quad (131)$$

Thus the frame-dragging profile along the strip direction is directly visible from the covariant strip inversion. By contrast, the lapse, radial scale, longitudinal spatial scale, and transverse warp factors remain mixed with  $W_x$  unless the transverse density is fixed by symmetry or separated using additional strip orientations.

The conclusion is therefore sharper than in the equal-time case. For an isotropic stationary strip, the transverse density is fixed by the common spatial warp factor, so the covariant strip data can reconstruct the undressed reduced stationary metric, including  $N(z)$ ,  $G(z)$ ,  $H(z)$ , and the shift  $v(z)$ , after the usual radial gauge choice. For an anisotropic stationary strip, one orientation reconstructs only the density-dressed block  $(\bar{A}_i, \bar{B}_i, \bar{C}_i)$  and the shift  $v_i = \bar{B}_i/\bar{A}_i$  along that direction. Recovering the undressed lapse and spatial warp factors requires separating the transverse densities  $W_i$ . With  $n = D - 2$  boundary spatial directions, this requires enough independent strip orientations to determine the  $n - 1$  relative anisotropy functions, together with one choice of common radial scale.

This classification can be stated more invariantly in terms of a simple rank-counting principle. The relevant number is not the spacetime dimension itself, but the number of gauge-

Table 1: Scope of the inversion formula. The controlling criterion is not the bulk dimension itself, but the comparison between the number  $N_{\text{unk}}$  of radial functions seen by the reduced HRT problem and the number  $N_{\text{data}}$  of independent coefficient functions supplied by the charge dependence of the HRT family.

Class	Representative metric sector	$N_{\text{unk}}$	$N_{\text{data}}$	Result
static equal-time radial sector	$ds^2 = z^{-2}[-N(z)^2 dt^2 + G(z)dz^2 + H(z)dx^2]$ , $\Delta t = 0$	1	1	one effective block
static covariant radial sector	$ds^2 = z^{-2}[-f(z)dt^2 + dz^2/f(z) + h(z)dx^2]$	2	2	closed if $B = 0$
3D stationary homogeneous sector	$ds^2 = z^{-2}[-f(z)dt^2 + dz^2/f(z) + h(z)(dx + v(z)dt)^2]$	3	3	closed: $f, h, v$
general 3D geometry	$ds^2 = g_{\mu\nu}(t, x, z)dx^\mu dx^\nu$	$\infty$	not fixed	not covered
higher-dimensional isotropic strip	$ds_{\text{sp}}^2 = G(z)dz^2 + H(z)\sum_i dx_i^2$	1 or 3	1 or 3	closed after reduction
higher-dimensional anisotropic strip, one orientation	$ds_{\text{sp}}^2 = G(z)dz^2 + \sum_i H_i(z)dx_i^2$	$> N_{\text{data}}$	1 or 3	density-dressed only
higher-dimensional anisotropic strips, all orientations	$ds_{\text{sp}}^2 = G(z)dz^2 + \sum_i H_i(z)dx_i^2$	depends	orientation-dependent	partial separation
stationary isotropic covariant strip	$W(z)^2[Gdz^2 - N^2 dt^2 + H(dx + vdt)^2]$	3	3	closed if $W$ fixed
stationary anisotropic covariant strip	$W_i(z)^2[Gdz^2 - N^2 dt^2 + H_i(dx_i + v_i dt)^2]$	$> 3$	3	partial: $\bar{A}_i, \bar{B}_i, \bar{C}_i$
higher-rank stationary sector	$n$ commuting Killing charges $p_I$ , $\Psi_{\bar{\kappa}} = \Gamma_{IJ}\kappa^I \kappa^J$	$\leq n(n+1)/2$	$n(n+1)/2$	Killing block
inhomogeneous geometry	$ds^2 = g_{\mu\nu}(z, x^i)dx^\mu dx^\nu$	$\infty$	not fixed	needs shape data
time-dependent geometry	$ds^2 = g_{\mu\nu}(t, z, x^i)dx^\mu dx^\nu$	$\infty$	not charge-based	not stationary
HRT phase transition	$S = \min_\alpha L_\alpha$	branch-dependent	branch-dependent	branchwise

inequivalent radial functions which remain after the HRT problem has been reduced to a one-dimensional radial variational problem. Let

$$N_{\text{unk}} = \text{number of radial functions seen by the chosen HRT family} \quad (132)$$

and let  $N_{\text{data}}$  denote the number of independent radial coefficient functions that can be extracted from the charge dependence of the reconstructed radial symbol. In the equal-time static problem there is only one effective charge direction, and the Abel inversion returns one coefficient function. This is the usual one-function inversion. In the covariant stationary three-dimensional problem there are two conserved endpoint charges,  $E$  and  $J$ , and the projective ratio  $\kappa = E/J$  makes the radial symbol a quadratic polynomial,  $\Psi_\kappa(z) = C(z) - 2\kappa B(z) - \kappa^2 A(z)$ . Thus the covariant interval data contain three independent coefficient functions. The present inversion therefore reconstructs the full stationary block, including the shift  $v_i$ . More generally, if a symmetry-reduced HRT problem has  $n$  independent conserved charges  $p_I$ , the charge dependence takes the form

$$\Psi_{\bar{\kappa}}(z) = \Gamma_{IJ}(z)\kappa^I \kappa^J, \quad \kappa^i = \frac{p_i}{p_n}, \quad \kappa^n = 1,$$

and the maximum number of radial coefficient functions available from a single smooth area-HRT branch is

$$N_{\text{data}} = \frac{n(n+1)}{2}.$$

The inversion is closed only when  $N_{\text{data}} \geq N_{\text{unk}}$ , after all gauge choices and density dressings have been accounted for. A fourth unknown function does not arise from the two-charge interval problem alone. It requires either additional independent probes, such as refined Rényi or source dependent data, additional strip orientations, or a higher-rank charge family. Table 1 summarizes the same statement in the examples considered below.

Table 1 summarizes what is and is not covered by the inversion formula. The formula applies to symmetry-reduced radial geometries, where a gauge choice has reduced the unknown metric functions to functions of the holographic coordinate alone. It does not apply to arbitrary three-dimensional metrics; time dependence, spatial inhomogeneity, and HRT branch changes require additional data beyond the one-dimensional Abel inversion.

The admissibility conditions are kinematic conditions on the HRT inversion, not bulk equations of motion. In the three-dimensional stationary homogeneous sector they test whether the holographic entanglement entropy can be represented by one radial metric block of the form (42). For a higher-dimensional strip, the same conditions test only the density-dressed block seen by the chosen strip orientation. Their failure therefore rules out that particular one-dimensional reduction, not necessarily the existence of a higher-dimensional bulk geometry. It may indicate that the transverse density has not been separated, that additional region shapes or strip orientations are needed, or that the physical entropy is mixing several HRT branches. Any further requirement that the reconstructed metric solve vacuum Einstein equations or an Einstein–matter system is a separate dynamical test, imposed after the characteristic inversion.

## 4 Examples

### 4.1 Pure AdS, rotating BTZ, and a static warped geometry

The previous sections derived the reconstruction formula, the cross-family compatibility conditions, and the causal readout of the reconstructed block. We now check the inverse map in examples where the entropy data can be written explicitly. The first two examples are worked reconstructions. Pure AdS fixes the normalization of the Abel variable and the radial coordinate. Rotating BTZ shows how the same sequence of steps reconstructs the stationary shift from the chiral thermal entropy. We then turn to examples that test the scope of the compatibility conditions.

**Pure AdS.** For the vacuum CFT on the line, the renormalized geodesic length is

$$L(\Delta t, \Delta x) = 2 \log \left( \frac{\sqrt{\Delta x^2 - \Delta t^2}}{\epsilon} \right), \quad \Delta x^2 > \Delta t^2, \quad (133)$$

up to an additive constant. Its endpoint derivatives are

$$E = -\partial_{\Delta t} L = \frac{2\Delta t}{\Delta x^2 - \Delta t^2}, \quad J = \partial_{\Delta x} L = \frac{2\Delta x}{\Delta x^2 - \Delta t^2}. \quad (134)$$

Thus

$$\kappa = \frac{E}{J} = \frac{\Delta t}{\Delta x}, \quad u_* = \frac{1}{J} = \frac{\Delta x^2 - \Delta t^2}{2\Delta x} = \frac{\Delta x}{2}(1 - \kappa^2). \quad (135)$$

Equivalently, along a fixed- $\kappa$  family,

$$\Delta x_\kappa(u_*) = \frac{2u_*}{1 - \kappa^2}, \quad \Delta t_\kappa(u_*) = \frac{2\kappa u_*}{1 - \kappa^2}. \quad (136)$$

The standard Poincare-AdS turning point is

$$z_* = \frac{1}{2} \sqrt{\Delta x^2 - \Delta t^2} = \frac{u_*}{\sqrt{1 - \kappa^2}}, \quad (137)$$

but in the inverse calculation this relation will be recovered from the Abel kernels rather than assumed.

For a fixed charge direction, the endpoint kernels are obtained by Abel inversion of the fixed- $\kappa$  separation data in (136). Explicitly,

$$T_\kappa(u) = \frac{1}{\pi} \frac{d}{du} \int_0^u \frac{u_* \Delta t_\kappa(u_*)}{\sqrt{u^2 - u_*^2}} du_* = \frac{\kappa u}{1 - \kappa^2}, \quad (138)$$

$$X_\kappa(u) = \frac{1}{\pi} \frac{d}{du} \int_0^u \frac{u_* \Delta x_\kappa(u_*)}{\sqrt{u^2 - u_*^2}} du_* = \frac{u}{1 - \kappa^2}. \quad (139)$$

The length kernel is obtained in the same way from the regulated length. Since

$$L_\kappa(u_*) = 2 \log \left( \frac{2u_*}{u_\epsilon} \right) + O(\epsilon^2), \quad u_\epsilon = \sqrt{1 - \kappa^2} \epsilon, \quad (140)$$

the Abel inverse gives

$$\begin{aligned} F_\kappa(u) &= \frac{1}{\pi} \frac{d}{du} \int_0^u \frac{L_\kappa(u_*)}{\sqrt{u^2 - u_*^2}} du_* \\ &= \frac{1}{\pi} \frac{d}{du} \left[ 2 \int_0^{\pi/2} \log \left( \frac{2u \sin \theta}{u_\epsilon} \right) d\theta \right] = \frac{1}{u}. \end{aligned} \quad (141)$$

Here the cutoff-dependent constant drops out after the final derivative. Thus the three pure-AdS kernels are obtained directly from the endpoint data.

The Abel kernels are naturally functions of  $u$ , but the metric is a function of the bulk radius  $z$ . The next step is therefore to reconstruct the map between these two variables. From the kernels we form

$$R_t(\kappa, u) = \frac{T_\kappa(u)}{F_\kappa(u)} = \frac{\kappa u^2}{1 - \kappa^2}, \quad R_x(\kappa, u) = \frac{X_\kappa(u)}{F_\kappa(u)} = \frac{u^2}{1 - \kappa^2}. \quad (142)$$

The characteristic derivative at fixed bulk radius is represented in  $(\kappa, u)$ -coordinates by

$$D_\kappa = \partial_\kappa - \frac{R_t}{u} \partial_u. \quad (143)$$

Acting on (142), it gives

$$D_\kappa R_t = \frac{u^2}{1 - \kappa^2}, \quad D_\kappa R_x = 0. \quad (144)$$

The radial-coordinate equation is then

$$Q = \frac{F_\kappa}{\sqrt{D_\kappa R_t}} = \frac{\sqrt{1 - \kappa^2}}{u^2}, \quad \partial_u \left( \frac{1}{z} \right) = -Q. \quad (145)$$

With the standard boundary normalization, this integrates to

$$z = \frac{u}{\sqrt{1 - \kappa^2}}. \quad (146)$$

It is useful to rewrite the reconstructed quantities in terms of this common radial coordinate. Pulling the kernels back to  $z$ -space gives

$$F_\kappa(z) = \frac{1}{z\sqrt{1 - \kappa^2}}, \quad T_\kappa(z) = \frac{\kappa z}{\sqrt{1 - \kappa^2}}, \quad X_\kappa(z) = \frac{z}{\sqrt{1 - \kappa^2}}. \quad (147)$$

More importantly, the ratios that enter the metric reconstruction become

$$R_t(\kappa, z) = \kappa z^2, \quad R_x(\kappa, z) = z^2. \quad (148)$$

Therefore the fixed-radius directional derivatives are simply

$$D_\kappa R_t = z^2, \quad D_\kappa R_x = 0. \quad (149)$$

Substitution into the local reconstruction formula gives

$$A = \frac{D_\kappa R_t}{z^2} = 1, \quad B = -\frac{D_\kappa R_x}{z^2} = 0, \quad C = \frac{R_x + \kappa R_t - \kappa^2 D_\kappa R_t}{z^2} = 1. \quad (150)$$

Consequently,

$$f = 1, \quad h = 1, \quad v = 0. \quad (151)$$

This example fixes the normalization of the radial coordinate and makes the logic of the reconstruction explicit: Abel inversion first gives  $F_\kappa, T_\kappa, X_\kappa$  as functions of the Abel variable  $u$ ; the radial-coordinate equation then converts  $u$  into  $z$ ; finally the  $z$ -space ratios  $R_t, R_x$  and their fixed-radius  $\kappa$ -derivatives give the metric block.

**Rotating BTZ.** We next repeat the same sequence for rotating BTZ, starting from the boundary entropy. Introduce chiral interval variables

$$\Delta x^+ = \Delta x + \Delta t, \quad \Delta x^- = \Delta x - \Delta t. \quad (152)$$

In units where the outer horizon is at  $z = 1$ , set

$$\alpha_+ = \frac{1 + \Omega}{2}, \quad \alpha_- = \frac{1 - \Omega}{2}. \quad (153)$$

The renormalized interval length is

$$L(\Delta t, \Delta x) = \log \left[ \frac{1}{\epsilon^2 \alpha_+ \alpha_-} \sinh(\alpha_+ \Delta x^+) \sinh(\alpha_- \Delta x^-) \right], \quad (154)$$

up to an additive normalization. Define

$$a_+ = \alpha_+ \coth(\alpha_+ \Delta x^+), \quad a_- = \alpha_- \coth(\alpha_- \Delta x^-). \quad (155)$$

Then

$$E = -\partial_{\Delta t} L = a_- - a_+, \quad J = \partial_{\Delta x} L = a_+ + a_-. \quad (156)$$

At fixed

$$\kappa = \frac{E}{J}, \quad u_* = \frac{1}{J}, \quad (157)$$

we have

$$a_+ = \frac{1 - \kappa}{2u_*}, \quad a_- = \frac{1 + \kappa}{2u_*}. \quad (158)$$

Solving (155) gives the one-parameter data

$$\Delta x_\kappa^+(u_*) = \frac{1}{\alpha_+} \operatorname{arctanh} \left( \frac{2\alpha_+ u_*}{1 - \kappa} \right), \quad (159)$$

$$\Delta x_\kappa^-(u_*) = \frac{1}{\alpha_-} \operatorname{arctanh} \left( \frac{2\alpha_- u_*}{1 + \kappa} \right). \quad (160)$$

The original time and space separations are

$$\Delta x_\kappa = \frac{1}{2}(\Delta x_\kappa^+ + \Delta x_\kappa^-), \quad \Delta t_\kappa = \frac{1}{2}(\Delta x_\kappa^+ - \Delta x_\kappa^-). \quad (161)$$

The chiral kernels are obtained by the same Abel inverse formula used in AdS case (138), (139). Applying this formula to (159) and (160), and using

$$\frac{1}{\pi} \frac{d}{du} \int_0^u \frac{u_* \operatorname{arctanh}(\lambda u_*)}{\sqrt{u^2 - u_*^2}} du_* = \frac{\lambda u}{2\sqrt{1 - \lambda^2 u^2}}, \quad (162)$$

we obtain

$$K_+(u) = \frac{1}{\pi} \frac{d}{du} \int_0^u \frac{u_* \Delta x_\kappa^+(u_*)}{\sqrt{u^2 - u_*^2}} du_* = \frac{u}{1 - \kappa} \left[ 1 - \left( \frac{2\alpha_+ u}{1 - \kappa} \right)^2 \right]^{-1/2}, \quad (163)$$

$$K_-(u) = \frac{1}{\pi} \frac{d}{du} \int_0^u \frac{u_* \Delta x_\kappa^-(u_*)}{\sqrt{u^2 - u_*^2}} du_* = \frac{u}{1 + \kappa} \left[ 1 - \left( \frac{2\alpha_- u}{1 + \kappa} \right)^2 \right]^{-1/2}, \quad (164)$$

where  $K_\pm$  corresponds to chiral inverse kernel for  $\Delta x_\kappa^\pm$  respectively. The physical time and space kernels are then

$$T_\kappa(u) = \frac{1}{2}(K_+(u) - K_-(u)), \quad X_\kappa(u) = \frac{1}{2}(K_+(u) + K_-(u)). \quad (165)$$

The length kernel is also obtained by Abel inversion. Along the same fixed- $\kappa$  family the length (154) becomes

$$\begin{aligned} L_\kappa(u_*) &= 2 \log \left( \frac{2u_*}{\epsilon \sqrt{1 - \kappa^2}} \right) - \frac{1}{2} \log \left[ 1 - \left( \frac{2\alpha_+ u_*}{1 - \kappa} \right)^2 \right] \\ &\quad - \frac{1}{2} \log \left[ 1 - \left( \frac{2\alpha_- u_*}{1 + \kappa} \right)^2 \right]. \end{aligned} \quad (166)$$

It is useful to separate the vacuum logarithmic term from the two finite thermal corrections. Define

$$\lambda_+ = \frac{2\alpha_+}{1 - \kappa}, \quad \lambda_- = \frac{2\alpha_-}{1 + \kappa}. \quad (167)$$

The Abel inverse of the vacuum logarithm is

$$F_\kappa^{\text{vac}}(u) = \frac{1}{\pi} \frac{d}{du} \int_0^u \frac{2 \log(2u_*/\epsilon \sqrt{1 - \kappa^2})}{\sqrt{u^2 - u_*^2}} du_* = \frac{1}{u}. \quad (168)$$

For each finite thermal correction we use

$$\frac{1}{\pi} \frac{d}{du} \int_0^u \frac{-\frac{1}{2} \log(1 - \lambda^2 u_*^2)}{\sqrt{u^2 - u_*^2}} du_* = \frac{1}{2u} \left( \frac{1}{\sqrt{1 - \lambda^2 u^2}} - 1 \right). \quad (169)$$

Therefore the full length kernel is

$$\begin{aligned} F_\kappa(u) &= \frac{1}{u} + \frac{1}{2u} \left[ (1 - \lambda_+^2 u^2)^{-1/2} - 1 \right] + \frac{1}{2u} \left[ (1 - \lambda_-^2 u^2)^{-1/2} - 1 \right] \\ &= \frac{1}{2u} \left[ \left( 1 - \left( \frac{2\alpha_+ u}{1 - \kappa} \right)^2 \right)^{-1/2} + \left( 1 - \left( \frac{2\alpha_- u}{1 + \kappa} \right)^2 \right)^{-1/2} \right]. \end{aligned} \quad (170)$$

Thus all three kernels  $F_\kappa, T_\kappa, X_\kappa$  have been obtained by Abel inversion from the fixed- $\kappa$  length and endpoint data. We first form the two ratios

$$R_t(\kappa, u) = \frac{T_\kappa(u)}{F_\kappa(u)}, \quad R_x(\kappa, u) = \frac{X_\kappa(u)}{F_\kappa(u)}. \quad (171)$$

At this stage the quantities  $R_t$  and  $R_x$  are functions of the Abel coordinate  $u$ . The metric functions, however, are functions of the bulk radial coordinate  $z$ . We therefore need the local change of variables between  $u$  and  $z$ . We use

$$D_\kappa = \partial_\kappa - \frac{R_t}{u} \partial_u, \quad Q = \frac{F_\kappa}{\sqrt{D_\kappa R_t}}, \quad \partial_u \left( \frac{1}{z} \right) = -Q. \quad (172)$$

Substituting the explicit BTZ kernels into  $R_t = T_\kappa/F_\kappa$  and  $R_x = X_\kappa/F_\kappa$ , and then applying  $D_\kappa$ , gives

$$Q(\kappa, u) = -\partial_u \left[ \frac{1}{u} \sqrt{\frac{d_\kappa + (1 + \Omega^2)u^2 + \sqrt{[d_\kappa + (1 + \Omega^2)u^2]^2 - 4u^2 [p_\kappa + \Omega^2 u^2]}}{2}} \right], \quad (173)$$

where

$$d_\kappa = 1 - \kappa^2, \quad p_\kappa = 1 + \Omega^2 + 2\kappa\Omega. \quad (174)$$

Thus the radial-coordinate equation integrates to

$$\frac{1}{z} = \frac{1}{u} \sqrt{\frac{d_\kappa + (1 + \Omega^2)u^2 + \sqrt{[d_\kappa + (1 + \Omega^2)u^2]^2 - 4u^2 [p_\kappa + \Omega^2 u^2]}}{2}}. \quad (175)$$

Equivalently,

$$z^2 = \frac{d_\kappa + (1 + \Omega^2)u^2 - \sqrt{[d_\kappa + (1 + \Omega^2)u^2]^2 - 4u^2 [p_\kappa + \Omega^2 u^2]}}{2 [p_\kappa + \Omega^2 u^2]}. \quad (176)$$

The sign is fixed by the asymptotic normalization

$$z \sim \frac{u}{\sqrt{1 - \kappa^2}} \quad (u \rightarrow 0). \quad (177)$$

The radial equation obtained from  $Q$  is more naturally used in the inverse form, as a map from the bulk radius to the Abel coordinate. Define

$$\Delta_\kappa(u) = [d_\kappa + (1 + \Omega^2)u^2]^2 - 4u^2 [p_\kappa + \Omega^2 u^2], \quad (178)$$

with

$$d_\kappa = 1 - \kappa^2, \quad p_\kappa = 1 + \Omega^2 + 2\kappa\Omega. \quad (179)$$

Substitution of the BTZ kernels into  $Q$  gives

$$Q(\kappa, u) = -\partial_u \left[ \frac{1}{u} \sqrt{\frac{d_\kappa + (1 + \Omega^2)u^2 + \sqrt{\Delta_\kappa(u)}}{2}} \right]. \quad (180)$$

For the BTZ kernels the radial-coordinate equation can be integrated in closed form<sup>3</sup>. It gives

$$\frac{1}{z} = \frac{1}{u} \sqrt{\frac{d_\kappa + (1 + \Omega^2)u^2 + \sqrt{\Delta_\kappa(u)}}{2}}, \quad (181)$$

<sup>3</sup>The algebraic relation between  $u$  and  $z$  in the BTZ example is a special simplification of the exact BTZ entropy. In a generic stationary radial geometry the same step is instead performed by solving the first-order relation  $\partial_u(1/z) = -Q(\kappa, u)$ , with the asymptotic normalization  $z \sim u/\sqrt{1 - \kappa^2}$ . Equivalently, near the boundary one may expand  $Q(\kappa, u) = \sqrt{1 - \kappa^2}/u^2 + q_0(\kappa) + q_1(\kappa)u + \dots$ , integrate to obtain  $z(u)$ , and then invert the resulting series locally. For example, if  $z(u) = u/a_\kappa[1 + q_0 u^2/a_\kappa + O(u^3)]$ , with  $a_\kappa = \sqrt{1 - \kappa^2}$ , then series reversion gives  $u(z) = a_\kappa z - q_0 a_\kappa^2 z^3 + O(z^4)$ .

where

$$\Delta_\kappa(u) = [d_\kappa + (1 + \Omega^2)u^2]^2 - 4u^2 [p_\kappa + \Omega^2 u^2], \quad (182)$$

and

$$d_\kappa = 1 - \kappa^2, \quad p_\kappa = 1 + \Omega^2 + 2\kappa\Omega. \quad (183)$$

To use the reconstruction formula, it is more convenient to rewrite this relation as  $u = u_\kappa(z)$ . Setting

$$y = u^2, \quad s = z^2, \quad b = 1 + \Omega^2, \quad (184)$$

equation (181) implies

$$\frac{1}{s} = \frac{d_\kappa + by + \sqrt{\Delta_\kappa(y)}}{2y}. \quad (185)$$

Hence

$$\sqrt{\Delta_\kappa(y)} = \frac{2y}{s} - d_\kappa - by. \quad (186)$$

Squaring this expression and using

$$\Delta_\kappa(y) = (d_\kappa + by)^2 - 4y(p_\kappa + \Omega^2 y) \quad (187)$$

gives

$$y(1 - bs + \Omega^2 s^2) = d_\kappa s - p_\kappa s^2. \quad (188)$$

Since

$$1 - bs + \Omega^2 s^2 = (1 - s)(1 - \Omega^2 s), \quad (189)$$

we obtain

$$u_\kappa(z)^2 = \frac{z^2 [d_\kappa - p_\kappa z^2]}{(1 - z^2)(1 - \Omega^2 z^2)} = \frac{z^2 [1 - \kappa^2 - (1 + \Omega^2 + 2\kappa\Omega)z^2]}{(1 - z^2)(1 - \Omega^2 z^2)}. \quad (190)$$

We now substitute the Abel-coordinate to the radial coordinate by

$$R_t(\kappa, z) = \frac{z^2(\kappa + \Omega z^2)}{(1 - z^2)(1 - \Omega^2 z^2)}, \quad (191)$$

$$R_x(\kappa, z) = z^2 \left[ 1 - \frac{\Omega^2 z^4 + \kappa\Omega z^2}{(1 - z^2)(1 - \Omega^2 z^2)} \right]. \quad (192)$$

Now  $D_\kappa$  has its intended meaning: it differentiates with respect to the charge direction while holding the bulk radius fixed. Therefore

$$D_\kappa R_t = \frac{z^2}{(1 - z^2)(1 - \Omega^2 z^2)}, \quad D_\kappa R_x = -\frac{\Omega z^4}{(1 - z^2)(1 - \Omega^2 z^2)}. \quad (193)$$

The first two inverse-block components are then

$$A = \frac{D_\kappa R_t}{z^2} = \frac{1}{(1 - z^2)(1 - \Omega^2 z^2)}, \quad B = -\frac{D_\kappa R_x}{z^2} = \frac{\Omega z^2}{(1 - z^2)(1 - \Omega^2 z^2)}. \quad (194)$$

The remaining component follows from the local algebraic formula:

$$C = \frac{R_x + \kappa R_t - \kappa^2 D_\kappa R_t}{z^2} = 1 - \frac{\Omega^2 z^4}{(1 - z^2)(1 - \Omega^2 z^2)}. \quad (195)$$

Finally,

$$f = \frac{1}{A} = (1 - z^2)(1 - \Omega^2 z^2), \quad v = \frac{B}{A} = \Omega z^2, \quad h = \frac{1}{C + B^2/A} = 1. \quad (196)$$

Equivalently, the frame-dragging profile is read directly from the directional variation of the endpoint response:

$$v(z) = -\frac{D_\kappa R_x}{D_\kappa R_t} = \Omega z^2. \quad (197)$$

Thus the rotating BTZ reconstruction follows the same pipeline as the pure-AdS check, but with a nonzero shift:

$$S_{\text{ren}} \longrightarrow K_\pm \longrightarrow T_\kappa, X_\kappa, F_\kappa \longrightarrow R_t, R_x \longrightarrow z(\kappa, u) \longrightarrow R_t(\kappa, z), R_x(\kappa, z) \longrightarrow A, B, C \longrightarrow f, h, v. \quad (198)$$

**A static warped geometry.** The first non-trivial example removes a common misconception: *rotation* is not the obstruction that prevents an equal-time inversion from determining the bulk metric. Even in a static three-dimensional geometry with a nontrivial spatial warp factor  $h(z) \neq 1$ , the equal-time entropy  $S(0, \Delta x)$  leaves  $f$  and  $h$  undetermined. Covariant interval data provide exactly the missing Hamilton–Jacobi direction.

To see this, recall that for a metric in the gauge (42) with  $v = 0$  but  $h(z) \neq 1$  the inverse-block functions are

$$A(z) = \frac{1}{f(z)}, \quad B(z) = 0, \quad C(z) = \frac{1}{h(z)}. \quad (199)$$

On the equal-time family  $\kappa = 0$  the optical turning point is

$$u_0(z) = z\sqrt{C(z)} = \frac{z}{\sqrt{h(z)}}, \quad (200)$$

so the length kernel involves only the combination  $\sqrt{A}/(zu'_0)$ , a single functional relation between  $A$  and  $C$ . This is the static two-function obstruction first identified in Section 2.2. In the covariant theory, by contrast,  $B = 0$  implies  $R_t = z^2\kappa A$  and the characteristic kernels give

$$z^2 A = D_\kappa R_t, \quad z^2 C = R_x. \quad (201)$$

The two radial functions are now separated by data, not by ansatz.

As a concrete toy model, take

$$f(z) = 1 - z^2, \quad h(z) = (1 + \beta z^2)^p, \quad v(z) = 0, \quad (202)$$

with  $\beta$  and  $p$  fixed constants. Then

$$A(z) = \frac{1}{1 - z^2}, \quad B(z) = 0, \quad C(z) = (1 + \beta z^2)^{-p}. \quad (203)$$

On the  $\kappa = 0$  family alone, the ratio data give

$$R_x(0, u_0) = u_0^2, \quad u_0(z) = \frac{z}{(1 + \beta z^2)^{p/2}}. \quad (204)$$

This identity does not reconstruct  $C(z)$  as a function of the bulk radial coordinate. It only defines the effective turning-point variable  $u_0$  seen by equal-time geodesics. To recover the warp factor  $C(z)$  itself, one must undo the relation  $u_0 = z\sqrt{C(z)}$ , which requires information from neighbouring fixed- $\kappa$  families.

The point of the covariant data is not merely to add another copy of the same equal-time relation. The equal-time data determine the Abel coordinate  $u_0$  and the equal-time length

kernel, but they do not determine how  $u_0$  is embedded into the bulk radial coordinate  $z$ . In the static case this can be seen directly. At  $\kappa = 0$ ,

$$R_x(0, u_0) = u_0^2, \quad u_0 = z\sqrt{C(z)},$$

so the equal-time endpoint response only says that the natural turning-point variable is  $u_0$ . It does not tell us separately what part of  $u_0$  came from  $z$  and what part came from  $C(z) = 1/h(z)$ .

The missing information appears in the first variation away from the equal-time family. Since  $B = 0$ , the covariant ratios have the local form

$$R_t(\kappa, z) = z^2\kappa A(z), \quad R_x(\kappa, z) = z^2C(z).$$

Hence, at fixed bulk radius,

$$D_\kappa R_t|_{\kappa=0} = z^2 A(z), \quad D_\kappa R_x|_{\kappa=0} = 0.$$

Thus the neighboring tilted HRT families supply precisely the radial lapse combination  $z^2 A$ , which is absent from the equal-time endpoint ratio.

Equivalently, the covariant data fix the map from the equal-time Abel variable to the actual bulk radius. Let  $F_0(u_0)$  denote the equal-time length kernel. The radial-coordinate equation at  $\kappa = 0$  reads

$$\partial_{u_0} \left( \frac{1}{z} \right) = - \frac{F_0(u_0)}{\sqrt{D_\kappa R_t(0, u_0)}}.$$

This equation is the step that equal-time inversion lacks: it determines  $z = z(u_0)$  on the chosen smooth branch. Once this map is known, the two radial functions are read off as

$$A(z) = \frac{D_\kappa R_t(0, z)}{z^2}, \quad C(z) = \frac{R_x(0, z)}{z^2}.$$

Equivalently,

$$f(z) = \frac{z^2}{D_\kappa R_t(0, z)}, \quad h(z) = \frac{z^2}{R_x(0, z)}.$$

For the toy profile (202), the equal-time variable is

$$u_0(z) = \frac{z}{(1 + \beta z^2)^{p/2}}, \quad R_x(0, z) = z^2(1 + \beta z^2)^{-p}.$$

The neighboring fixed- $\kappa$  data give

$$D_\kappa R_t(0, z) = \frac{z^2}{1 - z^2}.$$

Therefore the reconstruction gives

$$f(z) = \frac{z^2}{D_\kappa R_t(0, z)} = 1 - z^2, \quad h(z) = \frac{z^2}{R_x(0, z)} = (1 + \beta z^2)^p.$$

The warp factor is not obtained from the equal-time identity  $R_x(0, u_0) = u_0^2$  alone; it is obtained only after the covariant variation fixes the common radial coordinate and separates  $A$  from  $C$ .

The covariant time separation is therefore an essential part of the inverse data. Even at  $v = 0$ , the neighboring fixed- $\kappa$  families carry the second Hamilton–Jacobi direction needed to disentangle the radial lapse from the spatial warp. Rotation makes the additional shift function  $B$  nonzero; covariant data are then also needed to reconstruct  $g_{tx}$ , but they were already needed for  $h(z)$ .

## 4.2 A boosted Einstein–scalar black brane

We now give a non-BTZ example in which the scalar potential is fixed explicitly and the rotating geometry is known analytically. The example answers a narrow question: if a scalar condensate deforms the metric, does the characteristic inversion still reconstruct the deformed metric? The answer is yes, because the theorem is geometric. What is not determined by classical entanglement alone is the off-shell scalar potential away from the branch, unless a matter model is imposed.

Consider the three-dimensional Einstein–scalar action

$$I = \frac{1}{16\pi G} \int d^3x \sqrt{-g} \left[ R - \frac{1}{2}(\partial\phi)^2 - V(\phi) \right]. \quad (205)$$

For the potential

$$V(\phi) = -\frac{2(3 + 9s + 13s^2 - s^3)}{3(1 + s)^2}, \quad s := \tan^2 \frac{\phi}{2}, \quad (206)$$

one has the exact static solution

$$ds^2 = \frac{dr^2}{F(r)} + e^{2A(r)} [-F(r)d\tilde{t}^2 + d\tilde{x}^2], \quad (207)$$

$$A(r) = r - \frac{1}{2} \log(1 + e^{-2r}), \quad (208)$$

$$F(r) = 1 - \frac{2}{3}e^{-2r} - \frac{1}{3}e^{-4r}, \quad (209)$$

$$\phi(r) = 2 \arctan e^{-r}. \quad (210)$$

The AdS boundary lies at  $r \rightarrow \infty$ , where  $A(r) \sim r$ ,  $F(r) \rightarrow 1$ , and  $\phi \rightarrow 0$ . The horizon is at  $r = 0$ . Expanding the potential near the boundary gives

$$V(\phi) = -2 - \frac{1}{2}\phi^2 + O(\phi^4), \quad (211)$$

so the scalar saturates the three-dimensional Breitenlohner–Freedman (BF) bound,  $m^2 = -1$ . The branch is not a probe scalar placed on BTZ; it is a backreacted Einstein–scalar geometry. The same potential also admits the BTZ branch with  $\phi = 0$ .

The construction determines what can be inferred once the metric is known. In the domain-wall black-brane gauge

$$ds^2 = \frac{dr^2}{F(r)} + e^{2A(r)} [-F(r)dt^2 + dx^2], \quad (212)$$

the Einstein equations imply

$$\phi'(r)^2 = -2A''(r), \quad F''(r) + 2A'(r)F'(r) = 0, \quad (213)$$

and

$$V(\phi(r)) = -[F(A'' + 2A'^2) + A'F']. \quad (214)$$

For the functions in (208)–(210), these formulae reproduce (206). Hence, if the entropy inversion reconstructs the metric and one additionally assumes a minimal Einstein–scalar model in this gauge, the scalar magnitude and the potential along the solution curve can be reconstructed. The sign of  $\phi$  and the off-branch completion of  $V(\phi)$  are not fixed by entanglement alone.

A stationary rotating branch is obtained by a boundary boost,

$$\tilde{t} = \gamma(t - \omega x), \quad \tilde{x} = \gamma(x - \omega t), \quad \gamma = (1 - \omega^2)^{-1/2}. \quad (215)$$

The scalar remains  $\phi(r)$ , and the metric becomes

$$ds^2 = \frac{dr^2}{F(r)} + e^{2A(r)}\gamma^2[(-F + \omega^2)dt^2 + 2\omega(F - 1)dt dx + (1 - \omega^2 F)dx^2]. \quad (216)$$

For non-compact  $x$  this is a boosted black brane; after a quotient in  $x$  it is the direct analogue of a rotating branch. It solves the same Einstein–scalar equations because it is obtained by an isometry of the boundary directions before the quotient.

The causal-cone calculation is explicit. In the unboosted frame, requiring  $ds^2 = 0$ , the local projected null directions satisfy  $\frac{d\tilde{x}}{d\tilde{t}} = \pm\sqrt{F(r)}$ . Writing  $q = dx/dt$ , the boost gives

$$\frac{d\tilde{x}}{d\tilde{t}} = \frac{q - \omega}{1 - \omega q} = \pm\sqrt{F(r)}. \quad (217)$$

Thus the two characteristic roots in boundary coordinates are

$$q_{\pm}(r) = \frac{\omega \pm \sqrt{F(r)}}{1 \pm \omega\sqrt{F(r)}}. \quad (218)$$

They have the expected limits

$$q_{\pm}(\infty) = \pm 1, \quad q_+(0) = q_-(0) = \omega. \quad (219)$$

The ergosurface is the locus where  $g_{tt} = 0$ , namely

$$F(r_E) = \omega^2. \quad (220)$$

At the same point one of the two roots in (218) crosses zero. This reproduces, in a scalar-dressed geometry, the same interpretation found in rotating BTZ: the covariant entropy characteristic cone tracks the projected bulk light cone.

The comparison with BTZ is physically informative. The horizon generator is fixed by the boost parameter and is insensitive to the detailed scalar potential, whereas the location of the ergosurface depends on the full function  $F(r)$  and is therefore hair-sensitive. For a physical boost,  $|\omega| < 1$ . In that range  $\partial_t$  is timelike near the boundary, where  $F \rightarrow 1$ , but becomes spacelike near the horizon when  $\omega \neq 0$ . The surface  $F = \omega^2$  is therefore the ergosurface. When  $\omega = 0$ , it coincides with the horizon and there is no separate ergoregion. For  $|\omega| < 1$ , one has

$$0 < e^{-2r_E} < 1,$$

so the stationary-limit surface lies in the exterior region between the AdS boundary and the horizon  $e^{-2r_h} = 1$ . This is important because it shows that the cone roots distinguish two different pieces of rotating black-hole data: the horizon generator, obtained where the roots coalesce at  $F = 0$ , and the ergosurface, obtained where one projected root crosses  $q = 0$ . Thus the covariant entropy readout is sensitive not only to the horizon boost but also to the radial profile of the exterior ergoregion.

The projected cone roots in the boosted coordinates are

$$q_{\pm}(r) = \frac{\omega \pm \sqrt{F(r)}}{1 \pm \omega\sqrt{F(r)}}.$$

At the horizon  $F(r_h) = 0$ , the two roots coalesce to

$$q_+(r_h) = q_-(r_h) = \omega.$$

Thus the horizon-generator direction is fixed by the boost parameter, while the location of the ergosurface depends on the full radial profile of  $F(r)$ . Two boosted geometries with the same asymptotic boost can therefore share the same horizon-generator direction but have different ergoregion profiles. The entropy-side cone roots distinguish these two pieces of rotating black-hole data.

**Reconstruction of Scalar Potential** The characteristic inversion therefore reconstructs the deformed metric functions of (216). In a gauge of the form used in the main theorem, this is equivalently the reconstruction of the three inverse-block functions  $A, B, C$ , and hence of  $f, h, v$ . The scalar hair changes the radial dependence of the cone opening through  $F(r)$  and changes the radial gauge through  $A(r)$ . These changes are visible in the HRT length data. They are not visible as an independent scalar field unless further operator data or a matter model is supplied.

We distinguish two-stage inverse questions. The first is the geometric question studied in this paper,

$$S_{\text{ren}}(\Delta t, \Delta x) \implies g_{\mu\nu}(z). \quad (221)$$

The second is the dynamical compatibility question,

$$G_{\mu\nu}[g] - \frac{1}{2}g_{\mu\nu}R[g] = 8\pi G T_{\mu\nu}[\phi, V]. \quad (222)$$

Classical entanglement determines the left-hand side through the reconstructed metric. It does not by itself select a unique microscopic scalar field theory. If the minimal Einstein–scalar ansatz is imposed, equations such as (213) and (214) reconstruct  $\phi'(r)^2$  and  $V$  along the solution branch, but this is an additional dynamical assumption rather than a consequence of the area functional alone.

We now spell out how the characteristic metric reconstruction is followed by scalar-potential reconstruction once a minimal Einstein–scalar model is imposed. This calculation is not part of the purely geometric theorem; it is a dynamical refinement. The logic is

$$S_{\text{ren}}(\Delta t, \Delta x) \implies g_{\mu\nu}(r) \implies A(r), F(r) \implies \phi(r), V(\phi(r)), \quad (223)$$

where  $\theta = (\Delta t, \Delta x)$  denotes the boundary interval data. The last arrow uses the Einstein–scalar equations and is therefore conditional on the matter ansatz.

In the static rest frame the exact scalar branch of Section 4.2 is written as

$$ds^2 = \frac{dr^2}{F(r)} + e^{2A(r)} [-F(r)d\tilde{t}^2 + d\tilde{x}^2]. \quad (224)$$

For the action

$$I = \frac{1}{16\pi G} \int d^3x \sqrt{-g} \left[ R - \frac{1}{2}(\partial\phi)^2 - V(\phi) \right], \quad (225)$$

Einstein’s equations may be written as

$$R_{\mu\nu} = \frac{1}{2}\partial_\mu\phi\partial_\nu\phi + V(\phi)g_{\mu\nu}. \quad (226)$$

Substituting (224) gives three useful one-dimensional equations,

$$\phi'(r)^2 = -2A''(r), \quad (227)$$

$$F''(r) + 2A'(r)F'(r) = 0, \quad (228)$$

$$V(\phi(r)) = -[F(A'' + 2A'^2) + A'F']. \quad (229)$$

These identities determine the scalar magnitude and the potential along the solution branch from the reconstructed metric. Equation (227) determines  $|\phi'|$ . The sign of  $\phi'$  is fixed only after choosing a branch, for instance by demanding  $\phi \rightarrow 0$  at the AdS boundary and monotonicity toward the horizon. Equation (229) then gives the potential evaluated on that branch. If  $\phi(r)$  is monotonic, one may invert  $r = r(\phi)$  and obtain  $V(\phi)$  on the interval of field space probed by the solution.

For the explicit solution we take

$$A(r) = r - \frac{1}{2}\log(1 + e^{-2r}), \quad F(r) = 1 - \frac{2}{3}e^{-2r} - \frac{1}{3}e^{-4r}, \quad \phi(r) = 2\arctan e^{-r}. \quad (230)$$

Let

$$y = e^{-2r} = \tan^2 \frac{\phi}{2}. \quad (231)$$

Then

$$A'(r) = \frac{1+2y}{1+y}, \quad A''(r) = -\frac{2y}{(1+y)^2}, \quad (232)$$

and hence

$$-2A''(r) = \frac{4y}{(1+y)^2}. \quad (233)$$

On the other hand,

$$\phi'(r) = -\frac{2e^{-r}}{1+e^{-2r}}, \quad \phi'(r)^2 = \frac{4y}{(1+y)^2}. \quad (234)$$

Thus (227) is satisfied exactly. Furthermore,

$$F'(r) = \frac{4}{3}y(1+y), \quad F''(r) = -\frac{8}{3}y(1+2y), \quad (235)$$

and one verifies

$$F'' + 2A'F' = 0. \quad (236)$$

Finally, inserting (232) into (229) gives

$$V(r) = -\frac{2(3+9y+13y^2-y^3)}{3(1+y)^2}. \quad (237)$$

Since  $y = \tan^2(\phi/2)$ , the scalar potential reconstructed along the branch is

$$V(\phi) = -\frac{2(3+9s+13s^2-s^3)}{3(1+s)^2}, \quad s = \tan^2 \frac{\phi}{2}. \quad (238)$$

Near the AdS boundary,  $s \sim \phi^2/4$ , so

$$V(\phi) = -2 - \frac{1}{2}\phi^2 + O(\phi^4), \quad (239)$$

which corresponds to a scalar saturating the AdS<sub>3</sub> BF bound,  $m^2 = -1$ .

The boosted metric is

$$ds^2 = \frac{dr^2}{F(r)} + e^{2A(r)}\gamma^2 [(-F + \omega^2)dt^2 + 2\omega(F-1)dt dx + (1 - \omega^2 F)dx^2], \quad \gamma = (1 - \omega^2)^{-1/2}. \quad (240)$$

The scalar is still  $\phi = \phi(r)$  and the potential is still (238). The characteristic roots of the projected light cone are

$$q_{\pm}(r) = \frac{\omega \pm \sqrt{F(r)}}{1 \pm \omega \sqrt{F(r)}}. \quad (241)$$

They are read from the same covariant entropy characteristic cone that gives  $\kappa_{\pm}$ . At the boundary  $F \rightarrow 1$  and  $q_{\pm} \rightarrow \pm 1$ . At the horizon  $F = 0$  and  $q_+ = q_- = \omega$ .

If the entropy inversion reconstructs the metric, then  $F$  and  $A$  can be obtained explicitly. First, the horizon value of the root gives the boost parameter,

$$\omega = q_+(r_h) = q_-(r_h). \quad (242)$$

Then (241) gives

$$\sqrt{F(r)} = \frac{q_+(r) - \omega}{1 - \omega q_+(r)} = \frac{\omega - q_-(r)}{\omega q_-(r) - 1}. \quad (243)$$

Second, the determinant of the  $(t, x)$  block is boost invariant,

$$\det g_{ab}^{(t,x)} = -e^{4A(r)} F(r), \quad a, b = t, x. \quad (244)$$

Thus

$$e^{2A(r)} = \sqrt{-\frac{\det g_{ab}^{(t,x)}(r)}{F(r)}}. \quad (245)$$

The radial component then fixes the remaining radial parametrization. Once  $A(r)$  and  $F(r)$  are known in a rest-frame radial gauge, (227) and (229) reconstruct  $|\phi'|$  and  $V(\phi(r))$ . Applying these equations to (230) gives exactly (238). This shows explicitly how the geometric HRT inversion can be followed by a scalar-theory reconstruction, provided the minimal Einstein–scalar ansatz is imposed.

The boosted scalar example also provides a consistency check of the characteristic conditions themselves. Strip off the common conformal factor  $e^{2A(r)}$  from the  $(t, x)$  block in (240). The inverse block is

$$\mathcal{A}(r) = \frac{1 - \omega^2 F(r)}{F(r)(1 - \omega^2)}, \quad (246)$$

$$\mathcal{B}(r) = \frac{\omega(F(r) - 1)}{F(r)(1 - \omega^2)}, \quad (247)$$

$$\mathcal{C}(r) = \frac{F(r) - \omega^2}{F(r)(1 - \omega^2)}. \quad (248)$$

The characteristic ratios therefore have the same algebraic form as in the general theorem,

$$R_t = \rho(r)^2 (\kappa \mathcal{A} + \mathcal{B}), \quad R_x = \rho(r)^2 (\mathcal{C} - \kappa \mathcal{B}), \quad (249)$$

where  $\rho(r)$  denotes the radial prefactor used in the characteristic coordinate. The precise radial gauge is immaterial for the integrability check. Since  $D_\kappa$  is the derivative at fixed radius,

$$D_\kappa R_t = \rho(r)^2 \mathcal{A}(r), \quad D_\kappa R_x = -\rho(r)^2 \mathcal{B}(r), \quad (250)$$

and hence

$$D_\kappa^2 R_t = 0, \quad D_\kappa^2 R_x = 0. \quad (251)$$

Thus the exact rotating Einstein–scalar solution passes the same integrability test as rotating BTZ. The test is sensitive to stationarity and homogeneity, but not to the absence of scalar hair.

The same example clarifies how the horizon is identified from the entropy data. There are two equivalent local criteria. First, the projected causal cone degenerates:

$$q_+(r_h) = q_-(r_h). \quad (252)$$

For (241), this is exactly  $F(r_h) = 0$ . Second, in a gauge where the inverse block contains the usual blackening pole, the quantity  $D_\kappa R_t$  diverges because  $\mathcal{A} \sim 1/F$ :

$$D_\kappa R_t \longrightarrow \infty \quad (r \rightarrow r_h). \quad (253)$$

The first criterion is gauge-invariant in the projected causal block; the second is often the most direct consistency check in the reconstructed inverse block. Once  $r_h$  is located, the common value of the roots gives

$$\omega = q_+(r_h) = q_-(r_h). \quad (254)$$

The limitations are equally important. Classical entanglement determines the backreacted metric. It does not by itself distinguish  $\phi$  from  $-\phi$ , nor does it determine field redefinitions or the off-branch completion of  $V(\phi)$ . Those require additional matter-sector data, such as one-point functions, correlation functions, or a chosen scalar action.

### 4.3 A higher-dimensional strip degeneracy

The higher-dimensional strip discussion of Section 3.4 has a simple concrete meaning: a single strip orientation may not determine the undressed metric. We illustrate this with an explicit pair of geometries.

Consider a four-dimensional bulk equal-time spatial metric with two boundary spatial directions. Let

$$P = \frac{1}{z^2}.$$

The pure isotropic spatial metric is

$$ds_0^2 = \frac{1}{z^2} [dz^2 + dx^2 + dy^2]. \quad (255)$$

Now introduce a smooth anisotropy profile

$$\sigma(z) = \lambda \frac{z^2}{1 + z^2}, \quad (256)$$

and consider instead

$$ds_\lambda^2 = \frac{1}{z^2} [e^{2\sigma(z)} dz^2 + e^{2\sigma(z)} dx^2 + e^{-2\sigma(z)} dy^2]. \quad (257)$$

For  $\lambda \neq 0$ , this metric is anisotropic and is not the same as (255). Nevertheless, an  $x$ -oriented strip cannot distinguish the two.

Indeed, for a strip finite in  $x$  and extended along  $y$ , the strip data depend on

$$P_x(z) = z^{-2} \sqrt{H_x(z)H_y(z)}, \quad \Xi_x(P_x) = \sqrt{\frac{G(z)}{H_x(z)} \left| \frac{dz}{dP_x} \right|}.$$

For (255),

$$P_x = \frac{1}{z^2} = P, \quad \Xi_x = \frac{1}{2P^{3/2}}.$$

For (257), one has

$$H_x = e^{2\sigma}, \quad H_y = e^{-2\sigma}, \quad G = e^{2\sigma}.$$

Therefore

$$P_x = z^{-2} \sqrt{e^{2\sigma} e^{-2\sigma}} = P, \quad \Xi_x = \sqrt{\frac{e^{2\sigma}}{e^{2\sigma}} \left| \frac{dz}{dP} \right|} = \frac{1}{2P^{3/2}}.$$

Thus the two metrics give exactly the same  $x$ -strip Abel data, although their anisotropy profiles are different.

The degeneracy is not physical equivalence. It is a limitation of using only one strip orientation. A  $y$ -oriented strip sees instead

$$\Xi_y = \sqrt{\frac{G}{H_y} \left| \frac{dz}{dP} \right|} = \frac{e^{2\sigma(P)}}{2P^{3/2}},$$

and therefore distinguishes  $\lambda \neq 0$  from  $\lambda = 0$ . This explicit example is the only point needed here: in higher dimensions the strip entropy of one orientation reconstructs the density-dressed metric seen by that strip, not the full anisotropic spatial geometry. Additional orientations are needed if the transverse density is not fixed by symmetry.

**A time-dependent thin-shell obstruction.** The preceding examples were stationary: after the relevant symmetry reduction, the metric functions depended only on the radial coordinate. We now give a simple example showing how the admissibility conditions fail when this assumption is not true. The example is a thin-shell holographic quench, used only as an illustrative obstruction rather than as a full time-dependent HRT reconstruction.

A standard model is an AdS<sub>3</sub>-Vaidya geometry,

$$ds^2 = \frac{1}{z^2} [-f(v, z)dv^2 - 2dv dz + dx^2], \quad f(v, z) = 1 - m(v)z^2. \quad (258)$$

In the thin-shell limit one may take

$$m(v) = M\Theta(v). \quad (259)$$

Thus the geometry is pure AdS before the shell and BTZ after the shell. The shell represents the injection of energy in the boundary theory, and it breaks time-translation invariance. This is the essential difference from the stationary homogeneous geometries considered above.

For a boundary interval with endpoints

$$t_1 = T - \frac{\tau}{2}, \quad t_2 = T + \frac{\tau}{2}, \quad (260)$$

the parameter

$$\tau = t_2 - t_1 \quad (261)$$

is the time separation of the endpoints, while

$$T = \frac{t_1 + t_2}{2} \quad (262)$$

is the center time of the interval relative to the quench. In a stationary state, shifting both endpoints by the same amount would not change the HRT length, so the length would depend only on  $(\tau, x)$ . In the thin-shell state this is no longer true. Intervals with the same  $(\tau, x)$  but different  $T$  can lie before the shell, after the shell, or across the shell, and their HRT curves probe different bulk regions. The entropy therefore has the form

$$L = L(T, \tau, x), \quad (263)$$

not the stationary form  $L = L(\tau, x)$ .

This obstruction can be seen directly from the geodesic equations. For the Vaidya metric it is convenient to use the quadratic geodesic Lagrangian

$$\mathcal{L}_{\text{geo}} = \frac{1}{2z^2} [-f(v, z)\dot{v}^2 - 2\dot{v}\dot{z} + \dot{x}^2], \quad (264)$$

where the dot denotes differentiation along the geodesic. The  $x$ -direction remains homogeneous, and therefore

$$p_x = \frac{\partial \mathcal{L}_{\text{geo}}}{\partial \dot{x}} = \frac{\dot{x}}{z^2} \quad (265)$$

is conserved. This is the analogue of the spatial momentum  $J$ . By contrast, the momentum conjugate to  $v$ ,

$$p_v = \frac{\partial \mathcal{L}_{\text{geo}}}{\partial \dot{v}} = -\frac{f(v, z)\dot{v} + \dot{z}}{z^2}, \quad (266)$$

is not conserved, because the metric depends explicitly on  $v$ . Its evolution is

$$\frac{dp_v}{ds} = \frac{\partial \mathcal{L}_{\text{geo}}}{\partial v} = -\frac{1}{2z^2} \partial_v f(v, z) \dot{v}^2. \quad (267)$$

For the thin shell,

$$f(v, z) = 1 - M\Theta(v)z^2, \quad \partial_v f(v, z) = -Mz^2\delta(v), \quad (268)$$

and hence

$$\frac{dp_v}{ds} = \frac{M}{2} \delta(v) \dot{v}^2. \quad (269)$$

Thus the energy-like quantity jumps when the HRT curve crosses the shell. It is conserved separately in the pure-AdS region  $v < 0$  and in the BTZ region  $v > 0$ , but not across the shell. This is the explicit reason why the stationary Hamilton–Jacobi variables do not close. In a stationary geometry the endpoint derivative  $-\partial_\tau L$  can be identified with one conserved charge  $E$ , and the ratio  $\kappa = E/J$  labels the HRT family. In the thin-shell geometry there is still a conserved  $J$ , but there is no single conserved  $E$  along the whole curve. The value of the energy-like momentum before crossing the shell is not the value after crossing it.

The dependence on the center time  $T$  is the boundary manifestation of this jump. Shifting both endpoints by the same amount changes where the extremal curve meets the shell. Equivalently, the on-shell length is not invariant under a common shift of  $t_1$  and  $t_2$ . In the quadratic normalization above, the variation under such a common shift is controlled by the integrated non-conservation of  $p_v$ :

$$\frac{\partial L}{\partial T} \propto p_v|_2 - p_v|_1 = \int_\gamma ds \frac{\partial \mathcal{L}_{\text{geo}}}{\partial v} = \frac{M}{2} \int_\gamma ds \delta(v) \dot{v}^2. \quad (270)$$

The right-hand side vanishes only when the curve does not cross the shell. When the HRT curve intersects  $v = 0$ , the length changes with  $T$ . Therefore two intervals with the same  $(\tau, x)$  but different center time  $T$  need not have the same entropy.

## 5 Discussion

We have developed a local inverse formula for covariant holographic entanglement entropy beyond the one-coefficient equal-time inverse problem. The formula applies whenever the relevant Hubeny–Rangamani–Takayanagi (HRT) problem can be reduced, by symmetry and a radial gauge choice, to a one-dimensional radial problem with conserved endpoint charges. The input is the renormalized HRT length of spacelike boundary intervals,  $L(\Delta t, \Delta x) = 4G_N S_{\text{ren}}(\Delta t, \Delta x)$ . Its endpoint derivatives define the Hamilton–Jacobi data of the corresponding extremal curves. Hence, we can read an independent Hamiltonian–Jacobi direction from the two-variable dependence of the covariant, which is absent in equal-time entanglement. It provides a family of geometries for each fixed- $\kappa$ , and their consistency is precisely what allows one to reconstruct a single radial metric block.

Within the stationary homogeneous anti-de Sitter<sub>3</sub> (AdS<sub>3</sub>) metric class studied here, the entropy data determine the inverse block  $A, B, C$ , and hence the metric functions  $f, h, v$ , on the radial region swept out by the chosen smooth HRT family. The same construction also produces the local projected light cone,

$$\kappa_\pm(z) = -v(z) \pm \sqrt{f(z)/h(z)}.$$

This is a physical output of the covariant formulation. The reconstruction does not only recover a radial distance scale; it also recovers the tilt and opening of the stationary light cone in the

$(t, x)$ -plane. In rotating examples this gives a direct geometric meaning to the covariant interval data. The center of the cone is the frame-dragging profile, the closing of the cone locates the horizon generator, and the zero crossing of a projected root identifies the stationary-limit surface.

This interpretation also clarifies the relation to static inversions. In the static one-function limit the construction reduces to the familiar Abel-type logic of equal-time geodesic inversion. Once either a nontrivial spatial warp factor or a stationary shift is present, equal-time data alone no longer carry enough independent information. The time separation of the interval supplies the missing direction in boundary data. Equivalently, the different fixed- $\kappa$  families must agree on one common radial geometry. The resulting integrability condition is absent in a one-variable equal-time problem, and it is the new consistency requirement of the covariant stationary problem.

The examples illustrate the scope of the statement. Pure AdS gives the trivial light cone and reconstructs the undeformed radial block. Rotating Bañados–Teitelboim–Zanelli (BTZ) geometry shows how the chiral conformal-field-theory (CFT) entropy is reorganized by the inverse map into a radial frame-dragging profile and a projected causal cone. The boosted Einstein–scalar branch shows that the same causal readout is not restricted to locally AdS<sub>3</sub> quotients: two geometries may share the same horizon-generator direction while differing in the radial profile of the exterior ergoregion. Finally, the higher-dimensional strip example shows a limitation rather than a new closed theorem. A single strip orientation reconstructs only the density-dressed geometry seen by that strip. If the transverse density is not fixed by symmetry, additional orientations or shapes are needed. The thin-shell example gives a complementary obstruction: once the geometry depends on time, the entropy depends on the center time of the interval, and the stationary Hamilton–Jacobi charges are no longer globally conserved.

Several limitations are therefore intrinsic to the present result. First, the formula is not a reconstruction of arbitrary three-dimensional geometries. It assumes a stationary homogeneous radial problem and a gauge in which the unknown functions depend only on the holographic coordinate. Second, the reconstruction is branchwise. If the physical entropy is the lower envelope of several extremal surfaces, the formula applies only after a smooth HRT branch has been selected. Third, the theorem is kinematic. It reconstructs a classical metric block from the leading HRT area term. It does not by itself select a bulk matter model, a scalar potential, or a microscopic operator interpretation. Those questions require additional dynamical input, such as Einstein equations with specified matter content or independent CFT data. Fourth, quantum corrections are outside the classical formula unless the leading area contribution can be separated from bulk-entanglement corrections. Similarly, refined Rényi entropies involve cosmic-brane backreaction for  $n \neq 1$ , so their direct use requires a separate perturbative treatment around the reconstructed  $n = 1$  background.

The construction nevertheless has a practical advantage for holographic calculations. In many inverse problems one begins with a large ansatz for the bulk metric and then searches over functions numerically. The present formula reduces part of that search analytically. It identifies which combinations of entropy derivatives determine the radial block, which combinations must agree across fixed- $\kappa$  families, and which parts of the data cannot be interpreted within the assumed geometry class. Even when a full analytic inversion is not available, these relations can be used as constraints, consistency checks, or initial reductions before numerical reconstruction. The formula therefore reduces the effective number of unknown functions in practical holographic inverse problems, especially in stationary sectors where the covariant interval data are available.

A further structural extension is suggested by the branchwise nature of the present formula. In this work the inverse map is applied only after a smooth classical HRT branch has been selected. In a semiclassical treatment this restriction should be relaxed: the relevant extremal object is no longer only an area-extremizing surface, but a quantum extremal surface obtained from a generalized entropy functional. The corresponding inverse problem should therefore be

formulated not on a single smooth family of HRT curves, but on a branched space of candidate quantum extremal saddles. From this viewpoint, a Page transition is naturally interpreted as a change of branch in the geometric data from which the inverse map is constructed.

This suggests that the admissibility conditions can serve as a consistency test for the entropy data at the quantum level. In the classical problem, its second endpoint variation measures how the local bulk length data are distributed over the space of boundary intervals. In a quantum-corrected problem the same object should become branch-dependent: different quantum extremal saddles probe different portions of the bulk entanglement wedge, and the dominant contribution changes when the entanglement wedge changes. Thus the natural quantum extension of the present formula is not a second copy of the same Abel inversion. Rather, it is a branchwise tomographic problem in which the classical inverse map is applied separately on each smooth quantum extremal branch, while the transition loci encode how bulk information is reassigned between competing entanglement wedges.

This also points toward a more algebraic interpretation of the reconstruction. The finite-dimensional language of tensor-network bond dimensions is best understood as a regulated description of holographic encoding. In the continuum limit the relevant local algebras need not factorize in an ordinary Hilbert-space sense, and the appropriate notion of “capacity” should be expressed in terms of modular or relative-entropic data. The classical area density reconstructed in the present work may then be viewed as the leading semiclassical component of a more general entropy functional associated with the operator-algebraic encoding of the bulk.

In addition, there are several practical directions for future work. The first is to enlarge the class of symmetry-reduced HRT problems for which the characteristic Abel structure closes. The present derivation applies most directly when the HRT functional reduces to an effective radial problem. Higher-dimensional strips are the immediate testing ground: isotropic sectors close once the transverse density is fixed, while anisotropic sectors require additional orientations or shapes. A systematic classification of the minimal region data needed to separate these transverse densities would make the present scope statement into a practical reconstruction scheme. The second direction is numerical. Even when a complete analytic inversion is not available, the formula can reduce the number of unknown functions before a numerical search begins. One may reconstruct the effective radial block, impose the cross-family consistency conditions, and use any remaining mismatch to decide whether additional region data, transverse-density separation, or branch resolution is needed. The analytic formula can therefore provide a preliminary analytic reduction and a set of consistency conditions for more general numerical inverse holography.

## Acknowledgments

We especially thank Hun Jang, Hyun Seok Yang, and Keun Young Kim for their valuable comments and discussions.

## References

- [1] Juan Martin Maldacena. The Large N limit of superconformal field theories and supergravity. *Adv. Theor. Math. Phys.*, 2:231–252, 1998. doi: 10.1023/A:1026654312961.
- [2] S. S. Gubser, Igor R. Klebanov, and Alexander M. Polyakov. Gauge theory correlators from noncritical string theory. *Phys. Lett. B*, 428:105–114, 1998. doi: 10.1016/S0370-2693(98)00377-3.
- [3] Edward Witten. Anti-de Sitter space and holography. *Adv. Theor. Math. Phys.*, 2:253–291, 1998. doi: 10.4310/ATMP.1998.v2.n2.a2.

- [4] Shinsei Ryu and Tadashi Takayanagi. Holographic derivation of entanglement entropy from AdS/CFT. *Phys. Rev. Lett.*, 96:181602, 2006. doi: 10.1103/PhysRevLett.96.181602.
- [5] Veronika E. Hubeny, Mukund Rangamani, and Tadashi Takayanagi. A Covariant holographic entanglement entropy proposal. *JHEP*, 07:062, 2007. doi: 10.1088/1126-6708/2007/07/062.
- [6] John Hammersley. Extracting the bulk metric from boundary information in asymptotically AdS spacetimes. *JHEP*, 12:047, 2006. doi: 10.1088/1126-6708/2006/12/047.
- [7] John Hammersley. Numerical metric extraction in AdS/CFT. *Gen. Rel. Grav.*, 40:1619–1652, 2008. doi: 10.1007/s10714-007-0564-6.
- [8] Samuel Bilson. Extracting spacetimes using the AdS/CFT conjecture. *JHEP*, 08:073, 2008. doi: 10.1088/1126-6708/2008/08/073.
- [9] Samuel Bilson. Extracting Spacetimes using the AdS/CFT Conjecture: Part II. *JHEP*, 02:050, 2011. doi: 10.1007/JHEP02(2011)050.
- [10] Jaehyeok Huh and Chanyong Park. Dual gravities from entanglement entropy. 3 2026.
- [11] Veronika E. Hubeny, Hong Liu, and Mukund Rangamani. Bulk-cone singularities and signatures of horizon formation in AdS/CFT. *JHEP*, 01:009, 2007. doi: 10.1088/1126-6708/2007/01/009.
- [12] Netta Engelhardt and Gary T. Horowitz. Towards a Reconstruction of General Bulk Metrics. *Class. Quant. Grav.*, 34:015004, 2017. doi: 10.1088/1361-6382/34/1/015004.
- [13] Netta Engelhardt and Gary T. Horowitz. Recovering the spacetime metric from a holographic dual. *Adv. Theor. Math. Phys.*, 21:1635–1653, 2017. doi: 10.4310/ATMP.2017.v21.n7.a2.
- [14] Alex Hamilton, Daniel N. Kabat, Gilad Lifschytz, and David A. Lowe. Holographic representation of local bulk operators. *Phys. Rev. D*, 74:066009, 2006. doi: 10.1103/PhysRevD.74.066009.
- [15] Sebastian de Haro, Sergey N. Solodukhin, and Kostas Skenderis. Holographic reconstruction of space-time and renormalization in the AdS/CFT correspondence. *Commun. Math. Phys.*, 217:595–622, 2001. doi: 10.1007/s002200100381.
- [16] Vijay Balasubramanian, Borun D. Chowdhury, Bartłomiej Czech, Jan de Boer, and Michal P. Heller. Bulk curves from boundary data in holography. *Phys. Rev. D*, 89:086004, 2014. doi: 10.1103/PhysRevD.89.086004.
- [17] Bartłomiej Czech and Lampros Lamprou. Holographic definition of points and distances. *Phys. Rev. D*, 90:106005, 2014. doi: 10.1103/PhysRevD.90.106005.
- [18] Bartłomiej Czech, Lampros Lamprou, Samuel McCandlish, and James Sully. Integral Geometry and Holography. *JHEP*, 10:175, 2015. doi: 10.1007/JHEP10(2015)175.
- [19] Robert C. Myers, Junjie Rao, and Sotaro Sugishita. Holographic Holes in Higher Dimensions. *JHEP*, 06:044, 2014. doi: 10.1007/JHEP06(2014)044.
- [20] Michael Freedman and Matthew Headrick. Bit threads and holographic entanglement. *Commun. Math. Phys.*, 352:407–438, 2017. doi: 10.1007/s00220-016-2796-3.

- [21] Xi Dong, Daniel Harlow, and Aron C. Wall. Reconstruction of Bulk Operators within the Entanglement Wedge in Gauge-Gravity Duality. *Phys. Rev. Lett.*, 117:021601, 2016. doi: 10.1103/PhysRevLett.117.021601.
- [22] Koji Hashimoto. Building bulk from Wilson loops. *PTEP*, 2021(2):023B04, 2021. doi: 10.1093/ptep/ptaa183.
- [23] Koji Hashimoto and Ryota Watanabe. Bulk reconstruction of metrics inside black holes by complexity. *JHEP*, 09:165, 2021. doi: 10.1007/JHEP09(2021)165.
- [24] Wen-Bin Xu and Shao-Feng Wu. Reconstructing black hole exteriors and interiors using entanglement and complexity. *JHEP*, 07:083, 2023. doi: 10.1007/JHEP07(2023)083.
- [25] Daniel Kabat and Gilad Lifschytz. Emergence of spacetime from the algebra of total modular Hamiltonians. *JHEP*, 05:017, 2019. doi: 10.1007/JHEP05(2019)017.
- [26] Shubho R. Roy and Debajyoti Sarkar. Bulk metric reconstruction from boundary entanglement. *Phys. Rev. D*, 98:066017, 2018. doi: 10.1103/PhysRevD.98.066017.
- [27] Simon Caron-Huot. Holographic cameras: an eye for the bulk. *JHEP*, 03:047, 2023. doi: 10.1007/JHEP03(2023)047.
- [28] Ning Bao, ChunJun Cao, Sebastian Fischetti, and Cynthia Keeler. Towards Bulk Metric Reconstruction from Extremal Area Variations. *Class. Quant. Grav.*, 36:185002, 2019. doi: 10.1088/1361-6382/ab377f.
- [29] Niko Jokela, Tony Liimatainen, Miika Sarkkinen, and Leo Tzou. Bulk metric reconstruction from entanglement data via minimal surface area variations. *JHEP*, 10:079, 2025.
- [30] Byoungjoon Ahn, Hyun-Sik Jeong, Keun-Young Kim, and Kwan Yun. Holographic reconstruction of black hole spacetime: machine learning and entanglement entropy. *JHEP*, 01:025, 2025. doi: 10.1007/JHEP01(2025)025.
- [31] Sejin Kim. Learning the inverse Ryu–Takayanagi formula with transformers. *JHEP*, 04:128, 2026. doi: 10.1007/JHEP04(2026)128.
- [32] Bo-Wen Fan and Run-Qiu Yang. Application of Solving Inverse Scattering Problem in Holographic Bulk Reconstruction. *JHEP*, 03:044, 2026. doi: 10.1007/JHEP03(2026)044.
- [33] Zhenkang Lu, Cheng Ran, and Shao-feng Wu. Bulk Spacetime Encoding via Boundary Ambiguities. *Phys. Rev. Lett.*, 136(6):061603, 2026. doi: 10.1103/gmd3-zt39.
- [34] Zhenkang Lu, Cheng Ran, and Shao-feng Wu. Algebraic structure underlying pole-skipping points. *Phys. Rev. D*, 113(4):046008, 2026. doi: 10.1103/lgkz-gyll.
- [35] Guifre Vidal. Entanglement Renormalization. *Phys. Rev. Lett.*, 99:220405, 2007. doi: 10.1103/PhysRevLett.99.220405.
- [36] Guifre Vidal. Class of Quantum Many-Body States That Can Be Efficiently Simulated. *Phys. Rev. Lett.*, 101:110501, 2008. doi: 10.1103/PhysRevLett.101.110501.
- [37] Brian Swingle. Entanglement Renormalization and Holography. *Phys. Rev. D*, 86:065007, 2012. doi: 10.1103/PhysRevD.86.065007.
- [38] Mark Van Raamsdonk. Building up spacetime with quantum entanglement. *Gen. Rel. Grav.*, 42:2323–2329, 2010. doi: 10.1142/S0218271810018529.

- [39] Juan Maldacena and Leonard Susskind. Cool horizons for entangled black holes. *Fortsch. Phys.*, 61:781–811, 2013. doi: 10.1002/prop.201300020.
- [40] Ashley Milsted and Guifre Vidal. Geometric interpretation of the multi-scale entanglement renormalization ansatz. 2018.
- [41] Mukund Rangamani and Tadashi Takayanagi. *Holographic Entanglement Entropy*, volume 931 of *Lecture Notes in Physics*. Springer, 2017. doi: 10.1007/978-3-319-52573-0.
- [42] Aitor Lewkowycz and Juan Maldacena. Generalized gravitational entropy. *JHEP*, 08:090, 2013. doi: 10.1007/JHEP08(2013)090.
- [43] Thomas Faulkner, Aitor Lewkowycz, and Juan Maldacena. Quantum corrections to holographic entanglement entropy. *JHEP*, 11:074, 2013. doi: 10.1007/JHEP11(2013)074.
- [44] Netta Engelhardt and Aron C. Wall. Quantum Extremal Surfaces: Holographic Entanglement Entropy beyond the Classical Regime. *JHEP*, 01:073, 2015. doi: 10.1007/JHEP01(2015)073.
- [45] Xi Dong. The Gravity Dual of Renyi Entropy. *Nature Commun.*, 7:12472, 2016. doi: 10.1038/ncomms12472.
- [46] Koji Umemoto and Tadashi Takayanagi. Entanglement of purification through holographic duality. *Nature Phys.*, 14:573–577, 2018. doi: 10.1038/s41567-018-0075-2.
- [47] Phuc Nguyen, Trithep Devakul, Matthew G. Halbasch, Michael P. Zaletel, and Brian Swingle. Entanglement of purification: from spin chains to holography. *JHEP*, 01:098, 2018. doi: 10.1007/JHEP01(2018)098.
- [48] Souvik Dutta and Thomas Faulkner. A canonical purification for the entanglement wedge cross-section. *JHEP*, 03:178, 2021. doi: 10.1007/JHEP03(2021)178.
- [49] Maximo Banados, Claudio Teitelboim, and Jorge Zanelli. The Black hole in three-dimensional space-time. *Phys. Rev. Lett.*, 69:1849–1851, 1992. doi: 10.1103/PhysRevLett.69.1849.
- [50] J. David Brown and M. Henneaux. Central Charges in the Canonical Realization of Asymptotic Symmetries: An Example from Three-Dimensional Gravity. *Commun. Math. Phys.*, 104:207–226, 1986. doi: 10.1007/BF01211590.
- [51] Juan Martin Maldacena. Eternal black holes in anti-de Sitter. *JHEP*, 04:021, 2003. doi: 10.1088/1126-6708/2003/04/021.
- [52] David S. Berman and Maulik K. Parikh. Holography and Rotating AdS Black Holes. *Phys. Lett. B*, 463:168–173, 1999. doi: 10.1016/S0370-2693(99)00985-4.
- [53] David S. Berman. Aspects of holography and rotating AdS black holes. *PoS*, tmr99:008, 1999. doi: 10.22323/1.004.0008.
- [54] Ryusei Hamaki and Kengo Maeda. Semiclassical Rotating AdS Black Holes with Quantum Hair in Holography. *Phys. Rev. D*, 111:084021, 2025. doi: 10.1103/PhysRevD.111.084021.